POLITECNICO DI TORINO

Corso di Laurea Magistrale
in Ingegneria Biomedica

Tesi di Laurea Magistrale

Development of a novel 3D printed sensor for measuring joints flexion and extension

Relatore
Prof. Laura Gastaldi
Prof. Fabrizio Billi

Candidato
Filippo Zigliani

Anno Accademico 2018/2019

Abstract

Full knee range of motion (ROM) is one of the most important outcomes in patients after knee surgery, indeed full ROM is required for daily life activities and it is a fundamental condition for athletes before return to sport. Nowadays the most common techniques for measuring knee ROM include hand goniometers, electrogoniometers, inertial measurement units (IMU) and motion capture systems (MCS). However, these techniques usually remain constrained to specialized rehab center and require always the presence at least of one technician or physiotherapist. More recently there is an increasing interest in monitoring the patient also outside these facilities to obtain a bigger amount of data, to monitor patient's compliance and to improve the customization of the rehabilitation program. For all these reasons nowadays there is a major focus on developing wearable sensors that are light, low cost and low energy consuming.

This study aims to develop a novel, completely 3D printed wearable sensor that is capable of measuring knee ROM while it is embedded in garments. The novel sensor is completely built with a 3D printer combining conductive and non-conductive materials to create a resistive or a capacitive sensor. The resistive sensor exploits one conductive layer and works as a strain gauge that changes its resistance when it's stretched. The capacitive sensor instead is made of an alternation of conductive and non-conductive layers that create a parallel plate capacitor. When a strain occurs the distance between the layers and their sensing areas change causing a variation of capacitance. A total of 4 different models of the 3D printed sensors (1 resistive and 3 capacitive) were tested on a custom made machine to evaluate their stretchable properties. From this analysis, the best solution in terms of accuracy, low hysteresis, and more stretchability was a capacitive sensor made of 3 layers (2 conductive layers and 1 separation layer). The performance of this sensor were validated together with other 3 wearable commercial sensors (one flexible, one stretchable and IMUs) with a hand goniometer in a bending test on the knee of a subject.

The performance of the 3D printed stretchable sensor were validated also with the IMUs and the MCS in a gait and squat test. The root mean square error (RMSE) was calculated at the peaks of knee bending. The sensor showed promising results especially in the squat test validation, compared to IMUs and MCS an

RMSE of 4.26 degrees and 1.83 degrees respectively was recorded. Thanks to the promising results showed by the sensor and its features of lightness (less than 3 g) and low cost (less than 3 $) the 3D printed stretchable sensor can offer a valid alternative to the current methods for measuring joints ROM. With the possibility to embed the sensor in garments, both physiotherapists and patients can obtain continuous feedback on the rehabilitation process, offering the opportunity of programming a more precise rehabilitation protocol, following the daily activities of the patients. The combination of improved and optimized rehab regimens with increased patient engagement can be translated into a faster recovery and a lower healthcare cost.

Dedicated to my mother Cristina, my father Daniele
and my grandparents Antonino and Domenica.

Contents

List of Figures

List of Tables

List of Acronyms

ROM Range of motion

ACL Anterior cruciate ligament

TKA Total knee arthroplasty

IMU Inertial measurement unit

MCS Motion capture system

RS Resistive sensor

SCS Short capacitive sensor

LCS Long capacitive sensor

LTS Long thin sensor

VAS Visual analog scaler

IKDC International Knee Documentation Committee

TPU Thermoplastic polyurethane

PLA Polylactic acid

Chapter 1

Introduction

1.1 Knee range of motion and patient outcome

Range of motion (ROM) is a measurement of movement around a joint, in particular, knee ROM refers mostly to degrees of flexion and extension of the joint. Having a complete flexion and extension of the knee is a fundamental condition for the daily functions of the legs like walking, supporting body weight and balance control. Knee ROM includes passive ROM, active ROM and active assisted ROM. Passive ROM refers to how much the knee can be flexed or extended without the use of muscular strength but moved by an external force.

Active ROM instead is how much a patient can flex or extend his knee without any external force.

Active assisted ROM refers to how much the knee can be flexed or extended with some assistance. Early recovery of knee range of motion (ROM) is one of the most important goals to achieve in patients after anterior cruciate ligament (ACL) and total knee arthroplasty (TKA) surgery. Completely restored knee ROM is a fundamental condition to reach after a knee surgery since a loss of degrees in extension and flexion can cause abnormal gait, increase joint loading, cause patellofemoral pain, influence quadriceps strength and create a high prevalence of osteoarthritis [1]. Early recovery of ROM doesn't have negative effects as increasing effusion, hemarthrosis, periarticular soft tissue edema and swelling instead it can decrease the morbidity of major intraarticular ligamentous procedures [2] and increase the speed of the rehabilitation process. In particular, during the rehabilitation process patients are asked to achieve certain degrees of flexion or extension before performing precise exercises or before moving on the next phase of the rehabilitation protocol [3, 4, 5, 6, 1, 7]. Recover full ROM is also considered one of the most important goals fo athletes before returning to agonistic level sports [6, 8, 9, 10]. During the rehabilitation process, knee ROM is observed constantly and during every clinic visit to establish if the patient is improving his condition or if the rehabilitation exercises have caused swelling or pain that influence knee mobility.

1.1.1 Differences between bracing and non-bracing approaches and effect of early recovery of ROM

One of the most important phases of the rehabilitation process is restricted to the days right after surgery when the patient is still at the clinic. The approach of doctors and physiotherapists has changed during the years. In the past the approach was to immobilize the knee using chalk for long periods, then the braces were used to immobilize the joint for a short period. Nowadays the early recovery of ROM without using brace is preferred. There are still some debates on which is the best approach. Henriksonn et al.[11] conducted a study of two years follow up to compare the differences of patients who followed an early ROM rehabilitation protocol with patients whose knees were plaster immobilized. The braced group began ROM exercises from 7 days after surgery, the other group instead began after 4 weeks. They found no differences in either the sagittal knee laxity or the subjective function measured with the Lysholm score and the level of Tegner's activity between the two groups. They concluded that both treatments give the same results in terms of knee stability, subjective functions, and activity levels. Similar results were found by Risberg at al. [12] and Muellner et al. [13] which evaluated if the bracing the knee right after surgery produce benefits effects instead of a no bracing procedures. They discovered that the brace produces no differences in terms of knee joint laxity, range of motion, muscle strength, functional knee tests, patient satisfaction, or pain. Besides, they discovered that long term brace (1-2 years after surgery) produce weakness in the quadriceps muscle. On the other hand, a study conducted by Risberg at al. [12] found that the Cincinnati knee score, self-questionnaire to measure knee functions, was higher in the braced group, meaning that they had significantly improved knee function compared with patients in the non-braced group at the 3-month follow-up. The braced group instead showed higher atrophy compared with the non-braced patients after 3 months.

Noyes F. et al. [2] conducted a study to demonstrate that initiate knee ROM right after ACL reconstruction doesn't have negative effects like increasing effusion, hemarthrosis, periarticular soft-tissue edema, and swelling. The study was conducted on 18 patients, in 9 of them, knee ROM was initiated right after the surgery (10 hours of daily continuous passive ROM), in the other 9 subjects knee ROM was restricted at 10 degrees of flexion with a brace for the first 7 days. They found that initiate ROM right after ACLR doesn't have negative effects on the rehabilitation process (no stretching out the reconstructed or repaired ligament), instead, it decreases the morbidity of major intraarticular ligamentous procedures.

Noll S. et al. [1] in their study wanted to determinate a possible relationship between early side to side extension difference (4 weeks after surgery) and side to side extension after 12 weeks. Another aim was to evaluate the relationship between side to side difference and patient report outcomes for the International Knee Documentation Committee (IKDC) and visual analog scale (VAS). The data were collected after 4,8 and 12 weeks postoperative. The patients were asked to complete an IKDC and a VAS for pain at rest. Knee measurements were done with a goniometer on patients in a supine position. The results showed that there was a strong relationship between the patient's side to side knee extension difference after 4 and 12 weeks. A strong relationship was also found between the measurements done after 8 and 12 weeks. This study provides an initial goal of reaching 3-5 degrees of extension after 4 weeks postoperative and 2 degrees after 12 weeks. They concluded that the information that they provided with their study can be very helpful for clinicians and athletic patients that want to return quickly to sport.

S.van Grinsven et al. [4] underlined how important is to achieve at least 90 degrees of flexion in the first week after surgery, in particular, they suggest to focus the efforts on achieving full extension. In phase III (9-16 weeks after surgery) of the rehabilitation, they suggest the achievement of at least 130 degrees of flexion. Similar results have been found in another study conducted by Cavanaugh, J. T. et al [7] especially for restoring full ROM during phase III.

Bousquet B. et al. [3] focused their attention on ROM in phase I of the rehabilitation process (protective phase 0-6 weeks after surgery), when the passive ROM is $>$ 110 degrees the patient can progress in his rehabilitation beginning cycling without resistance. They stated that establish patellofemoral full ROM is important in the protective phase (phase I) and flexion is expected to be within 10 degrees of the opposite knee during phase I.

1.1.2 ROM outcome in rehabilitation protocols and return to sport requirements

Return to sport after ACL injury requires in general not less than 6 months, and there's not a single condition but a combination of requirements is asked to the patients before returning to practice sport. Several tests are used to detect patient performance: Single hop test, Isokinetic test, Single-leg triple crossover, Timed hop tests, Video drop-jump test, Single-leg squat test 0–90 degrees, Knee arthrometer test, Lachman, Pivot-shift tests, Knee examination (Range of knee motion, joint effusion, patellar mobility and crepitus)[14]. For what concern knee ROM, most of the studies requires full ROM as a condition to return to sport.

A study conducted by Kvist et al. [10] stated that objective criteria to return to sport are: full ROM and no pain or effusion, muscle strength and performance, static knee stability, social-physiological factors, and associated injuries. The majority of the test used on patients before returning to activities requires complete flexion and extension of the knee. For example Lentz. et al. [15] underlined the importance of ROM is in the single-legged Hop Testing, to perform this test full extension and active knee flexion within 5 degrees of the contralateral side is required.

After ACL surgery one important goal is to reach is the symmetrical ROM and performance, as stated by Shelbourne et al [16], since it allows to have better subjective and objective outcomes. Biggs et al. [6] focused their attention on the importance of restoring full symmetrical ROM regardless of the graft choice or the surgical procedure. This clinical commentary has the aim to create a new clinical model for ACL rehabilitation, the Knee Symmetry Model. ROM is measured on the patient in a supine position with a goniometer. The patient can initiate a pre-operative neuromuscular re-training as soon as ROM is improved. The study proposed a model with different goals to achieve during the rehabilitation process depending on the knee (graft donor knee or ACL reconstructed knee). For the ACL reconstructed knee patient is asked to flex and extend the knee four times per day. The goal of discharge from the hospital is to reach knee hyperextension and 125° knee flexion both symmetrically. For the Graft-Donor Knee (contralateral knee) the method addressed was the same used for an injured knee, knee hyperextension exercises were performed along with heel slide exercises for knee flexion. During the intermediate post-operative rehabilitation ACL, reconstructed knee exercises were aimed to improve both passive and active ROM. Patients were asked to monitor knee ROM during the second week after surgery. The most important goal in this phase is to continue the improvement of ROM to obtain symmetrical knee ROM. If there is pain or swelling the instructions are to reduce the strength of the exercises. On the Graft Donor Knee full ROM has to be achieved in the first week. One month after surgery the patient can participate in low impact activities such as the bike or elliptical trainer. The Knee Symmetry model offers then the possibility to the patients to restore normal knee ROM with predictable stability. Another beneficial factor of achieving symmetrical ROM is related to strength, in fact, patients that reach symmetrical ROM have better strength score. The study concluded that patients that reach symmetrical ROM have both better subjective and objective outcomes. The Knee symmetry model provides a means and description to reach these results. The key points of the rehabilitation program are: Elimination of time frames as post-operative guidelines, unrestricted ROM immediately, bed rest for the first week post-surgery and specialized rehabilitation for Graft donor and ACL reconstructed knee.

Even if some studies claim that certain outcomes are sufficient for release the return to sport confirmation, some studies affirm that there's a lack of objective criteria before return to athletics. A review conducted by Barber-Westin, S. D. et al [14] on the nowadays factors used to determinate when patient is available to return to sport after ACL reconstruction found that only the 13% (35) of the studies analyzed (264) noted objective criteria for return to sport (muscle strength or thigh circumference, general knee examination, single-leg hop tests, Lachman rating, or validated questionnaires) . ROM and effusion were found in 6% of the studies (15).

In opposition Shaw T. et al. [5] conducted a review on common outcomes used after ACL surgery in terms of reliability, validity, and sources of errors. After the review, recommendation measures were provided and relative time-frames during the rehabilitation period. For what concern ROM, they analyzed its importance not only as an outcome itself but also in his relationships to quadriceps strength. They confirmed that ROM is a fundamental outcome during the entire period of the rehabilitation process because it gives information about knee joint available range and possible interference made regarding neuro-muscular functions. This study stated that important time frames are 1-2 days, 2-4 and 3-6 months after surgery, in all of them ROM, together with VAS score for pain and SIRAS score, is considered a fundamental outcome.

1.1.3 Knee ROM measurement techniques

Knee ROM usually is measured on patients at the clinic during different phases of the rehabilitation process. The most common procedure to measure knee ROM is using a standard goniometer on the patient in a supine position on the clinic bed (see Figure 1.1). The patient is asked to bend his knee keeping the foot attached to the surface of the bed [18]. The physiotherapist documents both passive and active ROM in degrees. The center of the goniometer is positioned on the knee joint, the lateral malleolus at the ankle and the greater trochanter at the hip are the reference points. Another common technique is using the IMUs, usually two units are needed to detect knee ROM and these are fixed to the tight and the shank of the patient. Thanks to a support software usually sold with the units, is possible to detect not only flexion and extension but also abduction and adduction. Another very precise technique is the motion capture system, this is based on the use of camera and marker fixed on the body of the subject. The cameras are positioned around the entire shooting room to detect the movements of a subject even when he's not facing one of them.
All these sensors required the presence of specialists and physiotherapist and their value as monitoring tools remains constrained to the highly specialized lab, the clinic, or the rehab center. However, most of the patient's activities and most of the rehab regimen occur when the patient is outside these facilities missing an important opportunity to monitor compliance and better personalize the rehabilitation strategy. For this reason, nowadays there is an increasing interest in developing a wearable light and low cost sensor that can be used to measure and monitor joint activities. These types of devices are in general stretchable and flexible sensors made by conductive materials that detect strain or bending and correlate them

Figure 1.1: Knee hand goniometer

to the degrees of joint's bending. These sensors are usually light, low energy consumption and low cost. All these features allow the patients to bring home the sensors and consequently obtain data from everyday life activities. These data obtained during any time of the day offer feedback to both the patient and the physiotherapist involving an improvement in the rehabilitation approach. With the opportunity to record patient movements also when it is not at the clinic the rehabilitation process can be speeded up with precise exercises assigned depending on the daily activities of the patient. The aim of this master thesis project was to design a stretchable and flexible sensor, completely built on a 3D printer and insertable into garments, able to detect knee joint motion. The sensor was designed with the alternation of conductive and non-conductive materials to create resistive and capacitive sensors. One of this 3D printed stretchable sensor, together with other 3 commercial sensors, were validated with a hand goniometer on a subject's knee. The performance of the 3D printed sensor were also validated with both IMU and MCS in a squat and gait test.

Chapter 2

State of the art of stretchable and flexible sensors

2.1 Stretchable and flexible sensor structure

2.1.1 Resistive sensor materials and theoretical concepts

The two major groups of the flexible and stretchable sensors are the resistive and the capacitive sensors. Both of them work changing their values when they are stretched or flexed. From our current knowledge, there is not yet a gold standard material to build them. Resistive sensors are, in general, made by conductive stretchable fabrics that change their resistance while they are stretched or flexed. One of the first study found was conducted by Peter Gibbs and H. Harry Asada [19] in 2004 in which they developed a wearable conductive fiber that detects joint movement when is stretched. The conductive fiber is connected to a non-conductive flexible fabric and it passes over the joint on the top of the fabric. The other end of the fiber is attached to a coupled elastic cord, which is attached to the remote side of the joint. Therefore when there is a movement, any stretching takes place in the elastic cord and not in the conductive fiber. When there is a movement the cord changes his length and the conductive fiber slides pass a stationary wire contact. There is a permanent contact between the conductive fabric and the wire, and the resistance, which is linearly related to the length, is measured. In general resistive sensors exploit the concept used for the strain gauge, which according to the strain there is a change in the electrical resistance of the system. This concept was found in the study of Papi E. et al. [20] in which they developed a strain sensor made of graphitized carbon black nanopowder (20%) embedded in a polyurethane substrate (80%).

Sbernini L. et al. [21] in 2016 compared the performance of some of the currently available on the market flexible/stretchable sensor in measuring finger movements. The sensors were evaluated in terms of standard deviation and hysteresis.

The flexible sensors tested were different from each other especially for their coating. In particular, they were covered by polyester, polyamide and one non-coated. The polyester over-laminated RFSs was chosen as the most interesting sensors to be integrated into a sensory glove. The resistive sensors can also be made by piezoresistive fabrics as shown in the study of Tognetti et al. [22] with textile-based sensors produced using knitted piezoresistive fabrics (KPF) which contain 75% electro-conductive yarn (Belltron, produced by Kanebo Ltd) and 25% Lycra®. Also this sensor works changing its electrical resistance according to the strain. More in detail when a bi-component yarn of this type is elongated the interconnection between the fibers and stitches is modified by the application of a strain, causing a changing of the distance between the stitches and a changing of geometry interconnections of the fibers. Jiyong et al. [23] evaluated the performance of polypyrrole (PPy) conductive fabric to measure the flexion angle of the knee and elbow. Preliminary they discussed the anisotropic property of the materials (they tested 3 different compositions of PPy) that they have polymerized in situ. They made also tests to evaluate the change of the electrical resistance according to the flexion angle. They demonstrated that over 25% of elongation the resistance remains almost constant, concluding that the anisotropy feature of PPy conductive fabric resistance is dependent on the structure of the fabric itself.

Tien-Wei Shyr et al. [24] developed a similar device fixing a conductive strain sensor to a non-conductive and non-elastic webbing both on the side of the joint. Also in this case, they evicted the properties of the conductive material made of Polyamide fiber coated with carbon particles that change its resistance when it stretched. They found a good relationship between the angle and resistance with a linear relationship until 30% of stretching.

A different type of sensor but always resistive was designed by Sunghoon Ivan Lee et al. [25]. The sensor was based on a sensing unit attached to the tight and a string attached to the shank. There was a potentiometer that measured the number of rotations of a reel by changing resistance. The sensor works when the subject flex or extends his knee, the string pulls the reel and the potentiometer changes its resistance value, then the values are later converted to change of length of the string. During the flexion, the string increases its length and decrease consequently during the extension. This amount of change is then correlated to the degrees of bending of the joint analyzed.

More recently resistive sensors were directly made into garments without the encapsulating procedure into polymer materials to avoid problems such as low fit with the human body, unsatisfying comfort, and a complex preparation process. Yang Zhen et al. [26] in 2018 fabricated a graphene textile strain sensor without the encapsulating process into polymers demonstrating the more close-fitting whit the human's joints. More in detail the graphene textile was made of a conductive network with horizontal and vertical fibers. This type of textile can offer sensibility and long-term stability in a strain range of up to 15%.

Another application of graphene as a sensible element was found in a study conducted by Ju Ra Jeong et al. [27] in which the fabricated a highly stretchable strain sensor using a composite of graphene foam (GF) and PDMS. The GF was fragmented, grown before via chemical vapor deposition, into 200-300 μm sized fragments maintaining anyway the 3D structure of the GF. When a strain is applied the contact resistance between the contacting fragmented graphene foam surfaces change. The sensor is stretchable over 70% of his length with high durability over 10 000 stretching cycles with a high gauge factor.

2.1.2 Capacitive sensor materials and theoretical concepts

Capacitive sensors are also made as the resistive ones with conductive materials but they exploit more conductive layers to build one or more parallel plate capacitors. These type of sensors works detecting instead of the resistance of the single layers the changing of the capacitance of the entire system. Indeed capacitance depends on two main factors that can be altered during the stretching and the flexing of the capacitor, these are the area of the parallel plates and the distance between them. When a stretch/flex occurs on these sensor the area of the plate (which in the formula of capacitance is at the numerator) increase and the distance between the plate (which in the formula is at the denominator) decreases, the changing of both factors produce an increase of capacitance that can be correlated to the degrees of bending of human joints. Also in this case, there isn't a gold standard material or method to build one of these capacitive sensors.

A study conducted by Huang B. et al. [28] in 2017 designed a stretchable parallel plate capacitor sensible to the strain. The dielectric elastomer membrane was fabricated from a two-component silicone solution. To build the conductive layers they used graphite-elastomer composite. Totaro et al. in 2017 [29] developed sensorized wearable modules, for monitoring the movements of both knee and ankle joints. The sensors were two capacitors made of a combination of textile and elastic polymers. In particular, the bottom and top electrodes of the capacitor were connected to ground, while the central electrode provided the sensing signal to the conditioning electronics. In this way, parasitic capacitances and proximity effects were drastically reduced. The materials used for the conductive parts of the sensor was a stretchable conductive textile made by a combination of nylon and elastic fibers and plated in silver. For the dielectric layers, a silicone elastomer was used.

The same shape has been developed by Walker C. et al. [30] for measuring diver legs motion underwater. Also in this case the sensor was made with two capacitors with the upper conductive layers grounded, but the materials were, in this case, carbon-doped silicon mixture.

2.1.3 3D printed sensor

The type of sensors described above can be made also using a 3D printing technique, both capacitive and resistive sensors can be made. The main differences between the studies found are about the materials used to build the conductive part of the sensor.

One of the first studies was conducted by Alsharari M. et al. [31] in 2018 in which they designed a strain resistive sensor starting from graphene pellets and TPU flexible filament. The sensing part of the sensor was made drying first the graphene PLA pellets and then hot blended in a single screw extruder.

The same materials were used from Gul J. et al. [32] but in this case for both the part of the sensor (sensible and non-sensible) they started from TPU pellets, in the sensible part they inserted graphene pellets. The ratio of the concentration was not described in the study due to a pending patent.

Another example of a 3D printed sensor is in the capacitor sensor found in the study of Li K. et al. [33]. This study developed a coplanar capacitive sensor to detect not only strain but also pressure and tactile contacts. In this case, instead of graphene drugged TPU, carbon nanotubes (CNTs) were used as a conductive filler to prepare the printable ink. This choice was due to the advantage of the 1D nanostructure in terms of forming interconnected paths within the elastomer matrix. The preparation consisted of dispersing CNT powders homogeneously in a base made of PDMS. The final ratio of CNT/PDMS was 1/12 chosen because of the best electrical properties with less viscosity.

2.1.4 Calibration process and testing

Calibration procedures for stretchable and flexible sensors consist of correlating a change of resistance or capacitance, expressed in ohm or farad, to degrees of bending or percentage of strain depending on the application of the sensor. Different ways of testing and calibration have been found depending on the types of sensors. Even if a gold standard method was not found a lot of the studies included in this review did the calibration process with the help of motion capture systems (MCS).

For example, data can be acquired simultaneously from the sensor and camera motion capture system (MCS) [20, 25, 28] using a marker on the different sections of the lower limb to detect motions [30]. Thanks to the markers it is possible to recreate the 3D coordinates of the body joint's and calculate the angle of bending. Thanks to the time frame images it's possible to correlate the output signal (volts, ohms, farads, etc.) to the joint's motion and extract the transformation function. The subject can be asked to perform flexion and extension[28] (for examples from 90° to 0°), and both sensor and MCS output is detected. The main advantage of this technique is that is reliable and accurate but at the same time is expensive and requires opportune facilities.

Another common method to perform the calibration consist of using standard goniometer[19]. The procedure for measuring knee range of motion consists of using a long or short arm goniometer, the patient usually is asked to bend his knee every 10 degrees starting from maximum extension to maximum flexion. This technique can be less reliable than the camera-based but at the same time reduce the cost and the facilities needed for the calibration[34].

Some studies built their custom-made machines to test and calibrate the sensor depending on the joint that they want to analyze. These machines can simulate the movement for example of a finger and correlate the output values of the sensor to the degrees of bending of the joint like in the study conducted by Sbernini et al. [21]. The sensor was flexed thanks to a stepped motor and different percentages of flexing or stretching were tested. Another type of custom-made machine [24] used a protractor to record degrees of flexion and then they are correlated to the resistance values changes. In other cases, universal testing machines were used to test the stretching properties of the sensors [23, 31, 32]. The use of a universal machine is advantageous since it is reliable and is possible do perform repetitive cycles of strain with the same amount of force applied.

All the techniques described above refers only to test the sensors in terms of absolute performance. To consider a sensor solid, performance analysis that simulates everyday life or sports activities has to be performed. Most of these tests are performed on subjects that run, walk or other actions. Also in this case, different methods and performance-tests were found depending on the joint analyzed but also the different choices of the authors. Usually, to test the performance of the sensor the subject is asked to perform a walk, a squat or different type of movements and these are detected at the same time by reliable sensors such IMU sensors [22], MCS[20, 25, 28, 30],potentiometer[19] and goniometer together with the sensor tested. One common procedure is asking the subjects to bend his joint to certain degrees of flexion and detect the values from the sensors in different cycles and evaluate the results in terms of accuracy, precision, and hysteresis[21, 23]. In some cases instead the subject is asked to perform a squat[29], move their joint in precise positions[24, 30] or perform flexion/extension or abduction/adduction[19, 35]. Dynamic test can be performed like monopodalic standing characterized by slow knee flexion-extension movements [22] or walking/running treadmill tests[29, 25].

Chapter 3

Materials and Methods

3.1 Flexible sensor

The first sensor analyzed was purchased from Adafruit Industries (New York City, NY, USA) and it is a resistive flexible sensor (see Figure 3.1b). The sensor works changing its resistance when is bent in both directions. The range of resistance of the sensor is 10kΩ and the dimensions of the sensor are 112.5 mm/4.4 in of length, 6.38 mm/0.25 in of width, 0.5 mm/0.2 in of thickness, 0.5 g of weight.

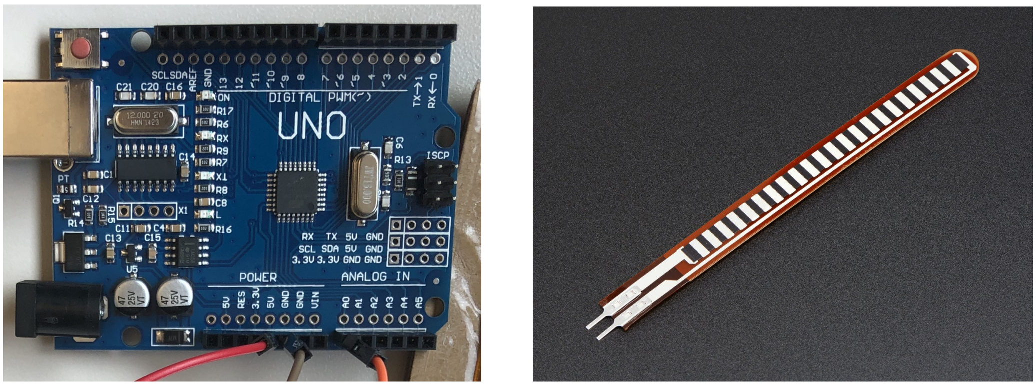

(a) (b)

Figure 3.1: Arduino UNO board and Adafruit flexible sensor.

The data were acquired with an Arduino UNO board (see Figure 3.1a), the change of resistance was detected with a voltage divider circuit built on a breadboard shown in Figure 3.4. The voltage used to power the circuit was 5 V and constant. The voltage divider circuit is based on two different resistors (one of these is the sensor) with similar values of resistance. The input voltage is split between the two resistors depending on their values. In this case, one resistance had a constant value of 20 kΩ and the other one (in this case the Adafruit sensor) had variable values. Exploiting this characteristic of variable resistance the voltage across the resistance of the sensor changes and thanks to the Arduino board is possible to detect this change of voltage.

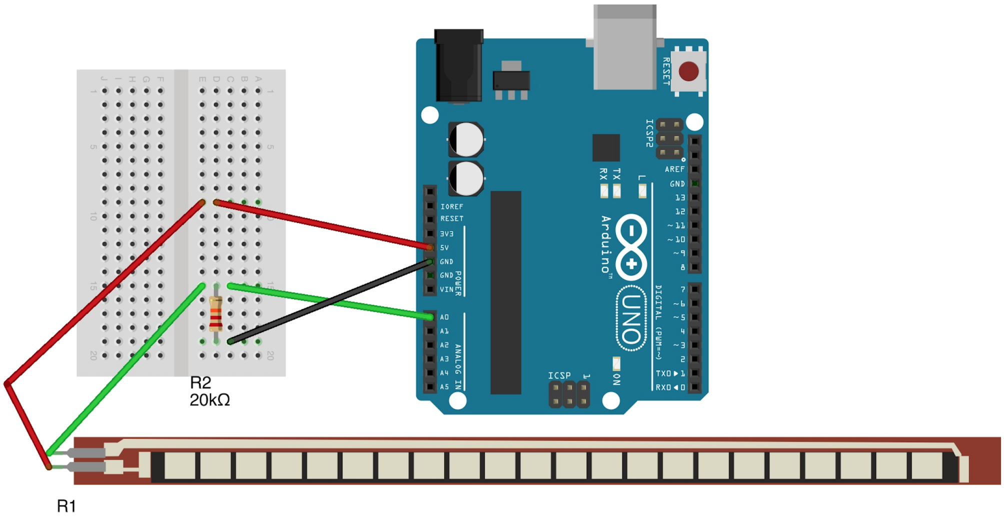

Figure 3.2: Arduino UNO board and voltage divider circuit connected to the Adafruit flexible sensor.

Figure 3.3: Adafruit sensor inserted into the custom made box on a soft knee brace.

The "analogRead" command was used in the code to convert the input voltage range, 0 to 5 volts, to a digital value between 0 and 1023 and it was performed by a circuit inside the microcontroller called an analog-to-digital converter or ADC. Figure 3.2 shows the Arduino UNO board and the relative connections with the breadboard that builds a voltage divider with the known value resistance R2 and the variable resistance of the sensor R1.

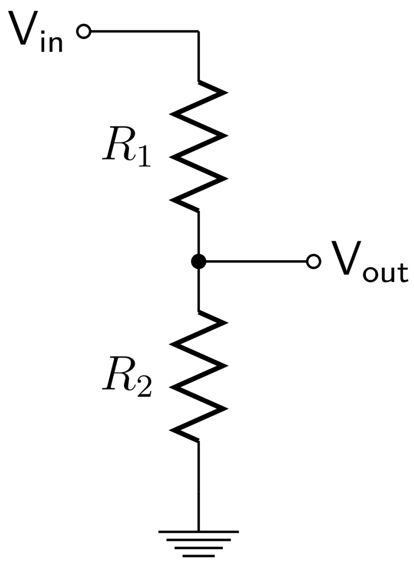

Figure 3.4: Voltage divider circuit where R2 has a fixed value and R1 is the flexible sensor.

The sensor was tested on a subject's knee in a bending test together with a hand goniometer. The subject was in a supine position and the hand goniometer was positioned on the knee of the subject following the written guidelines for measuring knee ROM [18]. The center of the goniometer was positioned on the knee joint, the lateral malleolus at the ankle and the greater trochanter at the hip were the reference points. Since the sensor was not able to stretch it was positioned inside a 3D printed box (see Figure 3.3) that made the sliding possible during the bending of the knee. The box was completely fixed on a wearable soft brace and only the upper part of the flexible sensor was fixed on the brace. During the bending then the sensor was able to slide inside the box but still able to measure the bending.

The subject was asked to bend his knee from 0 to 100 degrees at steps of 10 degrees. The correct angle of bending was measured by the hand goniometer and the Voltage values were recorded at the same time. Only the voltage values at the established degrees were recorded. The process was repeated for a total of 10 cycles, then the data were plotted with the voltage values to extract the calibration line. The line was then used to transform the voltage values in degrees of bending to compare them with the real angle of bending. The sensor was then evaluated in terms of standard deviation of measurements and accuracy, in particular, the distance from the "ideal" sensor line (in this case is a bisector in a graphs composed with expected degrees on the x-axis and measured degrees on the y-axis) was calculated in degrees and percentages of the range.

3.2 Stretchable sensor

The stretchable sensor analyzed in this study was purchased from Bendlab (Salt Lake City, UT, USA), and it can measure the angular displacement of the extremity of the sensor with a differential capacitance. The dimensions of the sensor are 100 mm x 7.62 mm x 1.27 mm (3.94 in x 0.30 in x 0.05 in) and it is made of medical-grade silicone elastomers doped with conductive and non-conductive fillers creating two capacitors. The sensor exploits differential capacitance measurement rejecting common-mode signals like temperature fluctuations, strain, and noise.

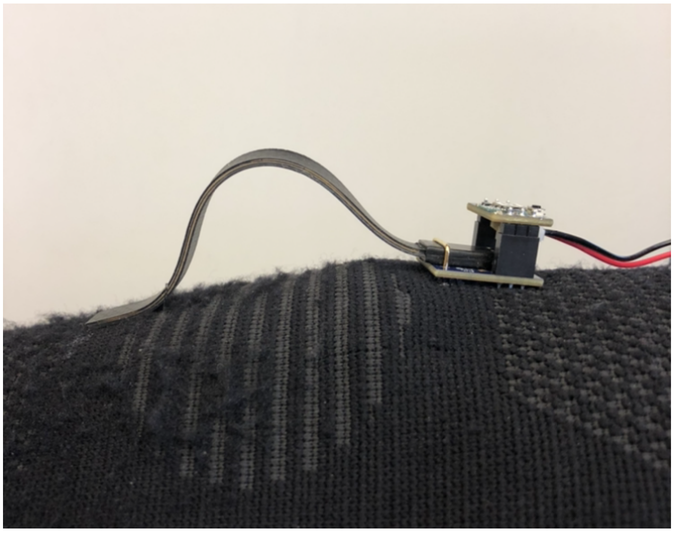

Figure 3.5: Bendlab sensor positioned on a soft knee brace.

The power consumption of this sensor is lower than 100 uA power at 1.8V. The sensor is designed to be path independent since it only measures the displacement between its two ending sections rejecting what happens between them. In particular, when it is bent in the midsections the two capacitors act differently since one experiences a compressive strain and the other a tensile strain. The sensor was accompanied by a lithium battery, a low-power integrated analog front end, an I2C interface, and a low energy Bluetooth stackable module. The sensor's company provides also a smartphone App able to record data and displays the angular displacements.

The sensor was positioned on the knee of a subject when the knee was bent, in this way the sensor was bent also when the knee was completely extended. This set up was chosen since the sensor was losing sensibility while it was stretched and flexed at the same time. With this set up shown in Figure 3.5 the sensor was working only flexing and not stretching itself.

For the Bendlab sensor, the same procedure as for the Adafruit sensor was used to test the sensor on the same subject's knee. Also in this case a total of 10 cycles were performed and the range was from 0 to 120 degrees at steps of 10 degrees. In this case, instead of the Arduino board, the smartphone App provided by the company was used to detect knee angles. The data were acquired first from the Bendlab App since the output was in degrees of bending. To reach a higher level of accuracy the degrees from the App were then recalibrated using a fitting equation. The procedure next was the same used for the Adafruit sensor and the results were compared in terms of standard deviation and accuracy calculated as distance from the "ideal" sensor line. Also in this case, the results are shown in degrees and percentages of the range.

3.3 IMU sensor analysis

The same procedure was used also on the IMUs, in particular, two units were positioned following the instruction of the Software iSen. The iSen software has different modes for measuring human body motion, the "lower limb" option was chosen with the "no feet" set up. This mode allows the knee motion detecting with the use of two IMUs positioned on the shank and the thigh of the subject. One sensor was positioned on the front side of the shank and the other one on the external side of the thigh (see Figure 3.6b). Also in this case, the subject was asked to bend his knee in a supine position for a total of 10 cycles. For the IMUs the calibration line was not used since the sensors were already calibrated for measuring knee motion, moreover, only the graphs with measured degrees and expected degrees will be shown. The performance, as done for the other sensors included in this study, were evaluated in term of accuracy.

3.4 3D printed stretchable sensor

Before testing the novel 3D printed stretchable sensor with the hand goniometer different models were tested in different stretching tests to choose the best one for measuring knee ROM. In particular, a total of 4 different models were tested and the best one in terms of reliability, accuracy and low hysteresis was chosen for the test with the hand goniometer. The best one was also validated in gait and squat tests with IMUs and MCS. Two different lengths were tested, the "short" sensors were 9.50 inches long and the "long" ones were 11.75 inches long. On the 4 sensors tested one was resistance based (RS) and the other 3 were capacitance-

(a) (b)

Figure 3.6: Example of a single unit of IMU and the positions required for detecting knee movements.

based (a short capacitive sensor (SCS), a long capacitive sensor (LCS) and a long thin capacitive sensor(LTS)). All these sensors were printed with a Prusa 3D printer equipped with a Multymaterial unit (MMU). Thanks to this equipment the printer was able to alternate non-conductive material (support for the sensor) and conductive material (sensible part of the sensor) in the same "Gcode" file. The models were created on INVENTOR software which was able to create a 3D model from a 2D sketch. The models were exported as ".stl" file and then imported in the PrusaSlicer software that translate a ".stl" file in "Gcode". The "Gcode" is a sequence of commands that include positions, speed, temperature and other commands that give instructions the nozzle of the 3D printer.

Each layer is printed perpendicularly to the previous one to improve the attachment between them. In this software, there is the possibility to change the settings of temperature, speed, layers' height, and others. The user can also decide the angle of the printing of the layers. Even changing the angle thought each layer will be printed perpendicularly to the previous one. If the user wants to change this setting, he has to modify the "Gcode" himself without the help of the software.

For each filament used, different settings were chosen depending on the composition of the materials. For example, printing a Polylactic acid filament (PLA) required a nozzle temperature between 180 and 215 Celsius degrees, for a Thermoplastic polyurethane (TPU) instead, a Temperature range of 230-240 Celsius degrees is preferred. In table 3.1 all the settings used to print the materials of the sensor are shown. In particular, for the support material, a TPU filament de-

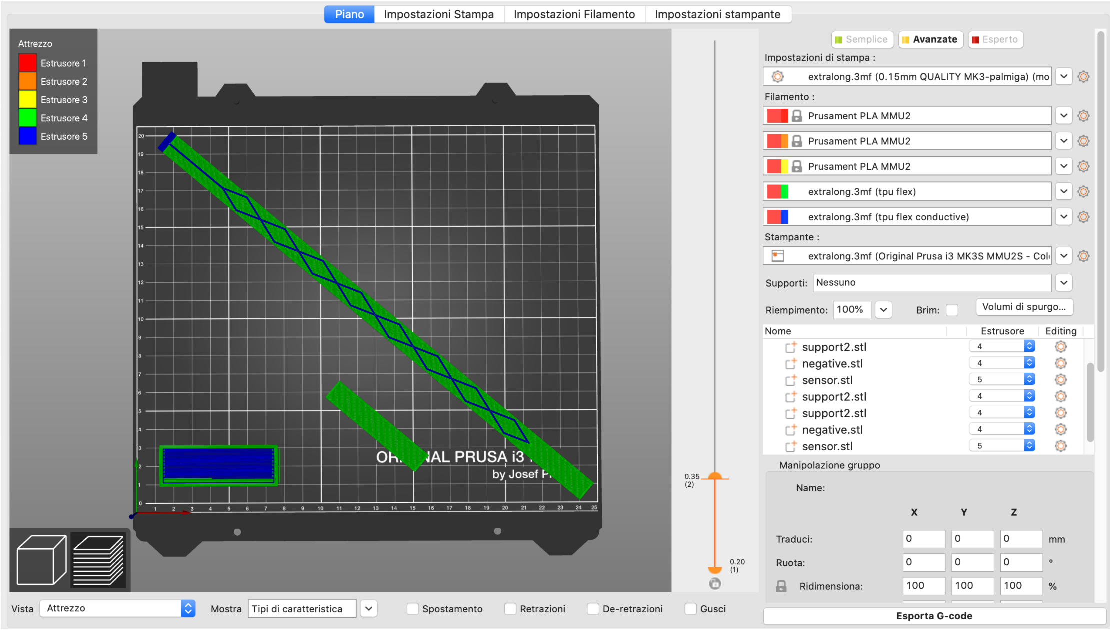

Figure 3.7: Capture took from the PrusaSlicer software with a sample of a 3D printed stretchable sensor.

signed by Ninjatek and purchased from Fenner Inc. (Manheim, PA, USA) was chosen. For the conductive material also TPU was used but drugged with graphene, this filament was also designed by Ninjatek with the name of Eel conductive filament. Another conductive filament was used and was purchased from CreativeTools (Halmstad, Sweden), also in this case, the material was TPU drugged with carbon fillers. Figure 3.7 shows an example of the settings used for printing one of the stretchable sensors tested in this study. It is possible to see on the main screen on the left the second layer of the sensor. The green sections refer to the TPU filament non-conductive while the blue is the TPU conductive filament. It is possible to see on the right of the image the settings for the single filament. Since in this case, only two filaments were used, only the extruder 4 and 5 were set up. In particular, extruder number 4 was used for the TPU non-conductive filament while the extruder number 5 for the TPU conductive filament. Below the settings for each extruder, all the layers are shown with the relative extruder. It is possible to see that the layer called “sensor”, which refers to the conductive pattern, is set up for filament 5 while the supports layers are set up with filament 4. On the plate of the 3D printer there are the sensor and 2 other rectangular objects. The one on the left is the default purge volume, it aims to clean the nozzle when the MMU changes the filament. Every time that the printer pass from one material to the other one layer of the purge is printed with the next material that had to be printed. It’s possible to choose the size of the purging volume depending on how much filament remains stuck in the nozzle. The second object was a secondary

Material Characteristic	**Palmiga TPU**	**Eel TPU**	**Ninjaflex TPU**
Conductive	yes	yes	no
Density	1.3 g/cm^3	-	-
Hardness	A 95	A 90	A 85
% Stretchable	250%	355%	660%
Diameter	1.75 mm	1.75 mm	1.75 mm
Price	82 $/kg	125 $/kg	85 $/kg
Printer settings	**Palmiga TPU**	**Eel TPU**	**Ninjaflex TPU**
Nozzle temperature	230°	230°	235°
Bed temperature	40	40	40
% Infill	100%	100%	100%
Speed	20 mm/s	20 mm/s	20 mm/s
Fan speed	0 mm/s	0 mm/s	0 mm/s
Layer thickness	0.15 mm	0.15 mm	0.15 mm

Table 3.1: Printer settings.

purge volume designed and positioned parallel to the sensor to recreate the pattern that needed to be printed for the support of the sensor. This purge volume, instead of changing materials every layer, was printed only with the TPU non-conductive. The second purge volume was chosen to be printed only with TPU non-conductive because the TPU conductive had the characteristic to remain more stuck in the nozzle than the TPU non-conductive. Some times also the operator needed to pause the printing process, pull out the TPU conductive, print some PLA to clean deeply the nozzle, load the TPU non-conductive and then restart the printing process. All these procedures are fundamental for the correct printing of the sensor. Indeed if there is some conductive material in the separation layer it can short the circuit and avoid the building of the parallel plate capacitor. Moreover, to print correctly the sensor and avoid damage during the pulling off procedure from the bed, the surface of the bed was covered with a common glue stick, in this way the sensor didn't stick directly to the bed and was easier to remove.

3.4.1 3D printed sensors dimensions and theoretical concepts

All the 3D printed sensor signals were filtered with a Kalman Filter. This is a recursive filter that is used for dynamic systems. The Kalman filter used in the Arduino code could be set up depending on the range of the noise. Equation 3.1 explains how the Kalman filter works, the operator can set up the values of *Emeasure* and q where the first one refers to the range of the noise and the second one is a values between 0 and 1, the more q is low the more the filter attenuates the signal. On the other hand, q has not to be too low otherwise the response of the signal is slow. For the resistive sensor 100000 as $Emeasure$ and 0.1 as q was set up, for the capacitive sensors instead 5 as $Emeasure$ and 0.1 as q.

$$\begin{gathered}
Kgain = Estimate/(Estimate + Emeasure) \\
Cestimate = Lestimate + Kgain * (Emeasure - Lestimate) \\
Estimate = (1.0 - Kgain) * Estimate + fabs(Lestimate - Cestimate) * q \\
Lestimate = Cestimate \\
return(Cestimate)
\end{gathered} \tag{3.1}$$

The RS (see Figure 3.11a) works as a strain gauge that changes its electrical resistance when is stretched. For all the sensors included in this study, the shape was designed to reproduce the behavior of a spring. More in detail the shape (for the conductive material) was made of a sequence of rhombus all connected. This shape allows the sensor to be more stretchable. For the resistive sensor a total of three layers were printed, the first one and the last one are only made of TPU non-conductive (support layers), the mid-layer instead has both TPU conductive and non-conductive material. In particular, the holes inside the rhombus and the parts outside them are filled with the TPU non-conductive. For this resistive

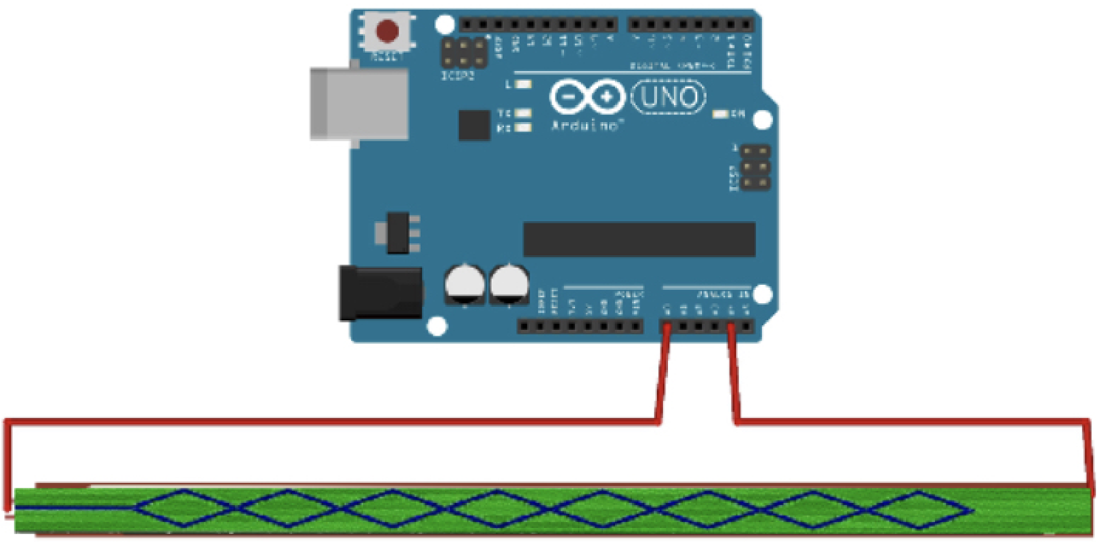

Figure 3.8: Arduino UNO and relatives connection with a model of 3D printed stretchable sensor.

sensor also an Arduino UNO board (see Figure 3.8) was used to detect the change of resistance. Also in this case, a voltage divider was built on a breadboard, but the fixed resistor had 1MΩ as electrical resistance since the resistance values of this sensor started at 500 kΩ when it is non-stretched until 100 kΩ when it is stretched. The resistive sensor is 9.50 inches (24.1 cm) long and 0.017 inches (0.45 mm) thick, the conductive section as described before is made of rhombi, in particular, the minor axis of the rhombus is 0.31 inches (8 mm) and the major is 0.94 inches (16 mm). Figure 3.9 shows the two different sizes of the 3D printed sensors. For

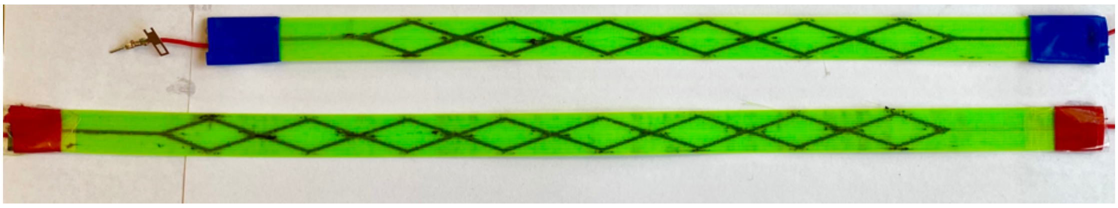

Figure 3.9: Two sizes of the 3D printed sensors, the upper sensor is 9.50 inches long and the lower is 11.75 inches long.

the capacitive sensors (SCS, LCS, and LTS) instead, the working principle of a parallel plate capacitor was exploited alternating conductive and non-conductive layers.When a stretching occurs the two conductive layers get closer to each other and at the same time the area that faces the gap between them increases (see Equation 3.4 where "C" is capacitance, "ϵ" is the permittivity of the dielectric, "A" is the area of the plates overlap and "d" is the distance between them).

$$C = \frac{\epsilon A}{d} \tag{3.2}$$

The Arduino UNO board was used to detect the change of capacitance. The internal capacitor which is connected to the ground (C2) of the Arduino board was used as a known capacitor (range from 20 to 30 pF) and the capacitive sensors were used as an unknown capacitor (C1) in a capacitive voltage divider. Thanks to the detecting of the change of voltage it was possible to extract the change of capacitance of the sensor (see Equation 3.3). Figure 3.10 shows the circuit diagram of the capacitance-voltage divider where C1 is the Arduino UNO internal capacitance connected to ground and C2 is the capacitive sensor.

$$Vout = \frac{Vin \cdot C1}{C1 + C2} \tag{3.3}$$

The SCS (see Figure 3.11b) is made of 5 layers, 2 of them contains the conductive patterns, the top and the lowest ones work as supports and the mid one works as a separation layer. The only dimension that changes from the RS sensor is the thickness, in this case, is 0.029 inches (0.750 mm).

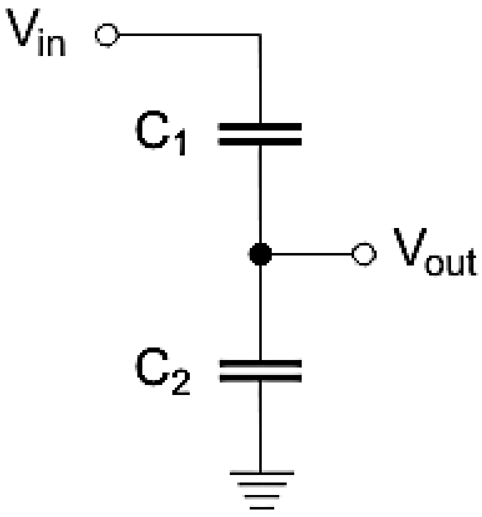

Figure 3.10: Capacitance voltage divider.

The LCS (see Figure 3.12a) was designed with the same shape used for the SCS but longer, indeed instead of having 6 rhombi connected it has 8 rhombi. In this sensor 2 layers of separation were used for a total of 6 layers (2 support layers, 2 separation layers, and 2 conductive layers). The total thickness of the sensor is 0.035 inches (0.900 mm) and is 11.75 inches long (29.85 cm).

Finally, the LTS (see Figure 3.12b) was designed with the same dimension of the LCS but only 1 separation layer was used and no support layers were added. This choice was due to the intent to make the sensor as stretchable as possible. The LTS sensor has in total 3 layers which means a total thickness of 0.017 inches (0.45 mm), this implicates that the conductive patterns of the sensor are exposed to the air. Table 3.2 summarize all the features of the 3D printed sensors.

	Sensor 1	**Sensor 2**	**Sensor 3**	**Sensor 4**
Acr.	RS	SCS	LCS	LTS
Resitive	x	-	-	-
Capacitive	-	x	x	x
Length	9.5 in	9.5 in	11.75 in	11.75 in
N. Layers	3	5	6	3
Disposition	S,C,S	S,C,S,C,S	S,C,S,S,C,S	C,S,C

Table 3.2: Features of the four 3D printed stretchable sensors, in particular the “x” refers if the sensor is resistance-based or capacitance-based, the disposition indicates the order of S(support non-conductive layer) and C(conductive layer).

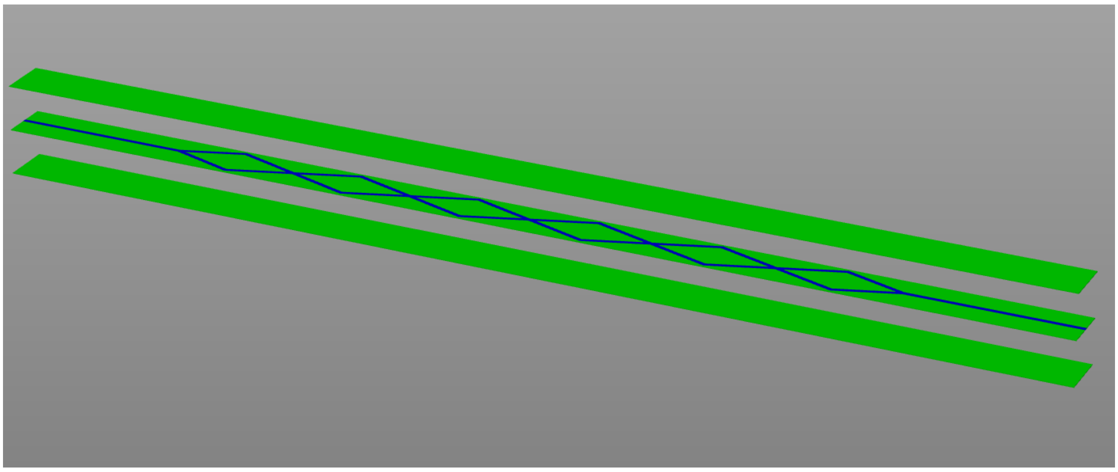

(a)

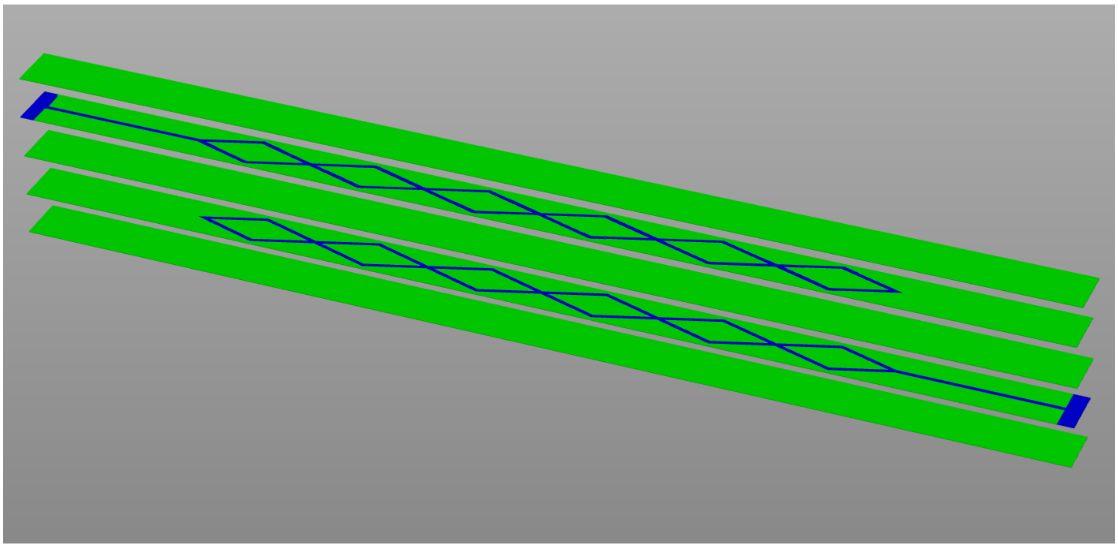

(b)

Figure 3.11: RS and SCS sensors.

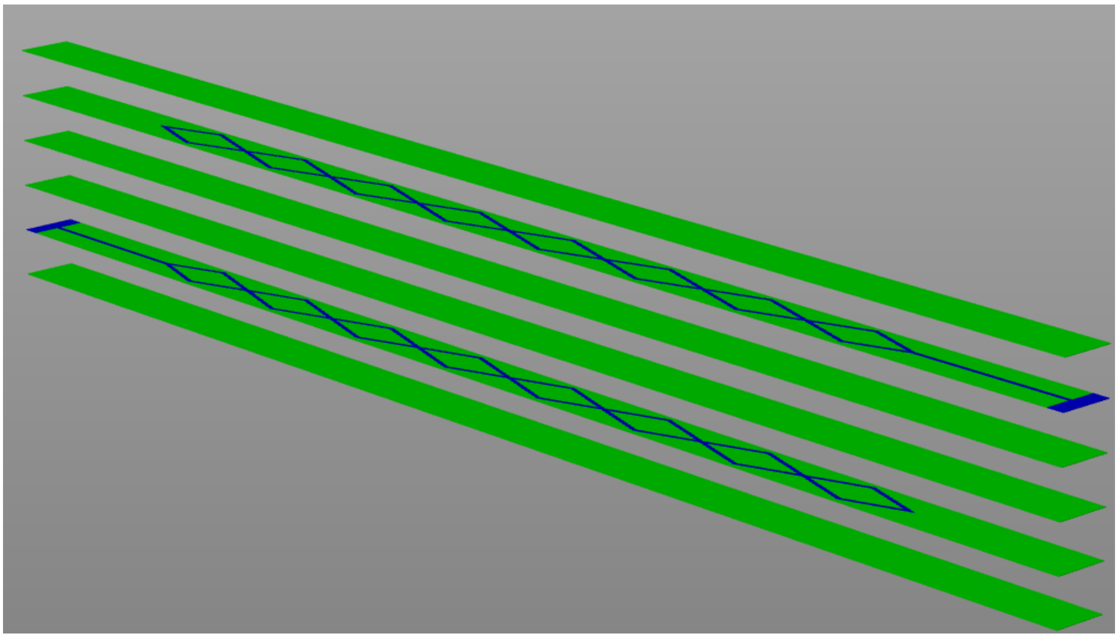

(a)

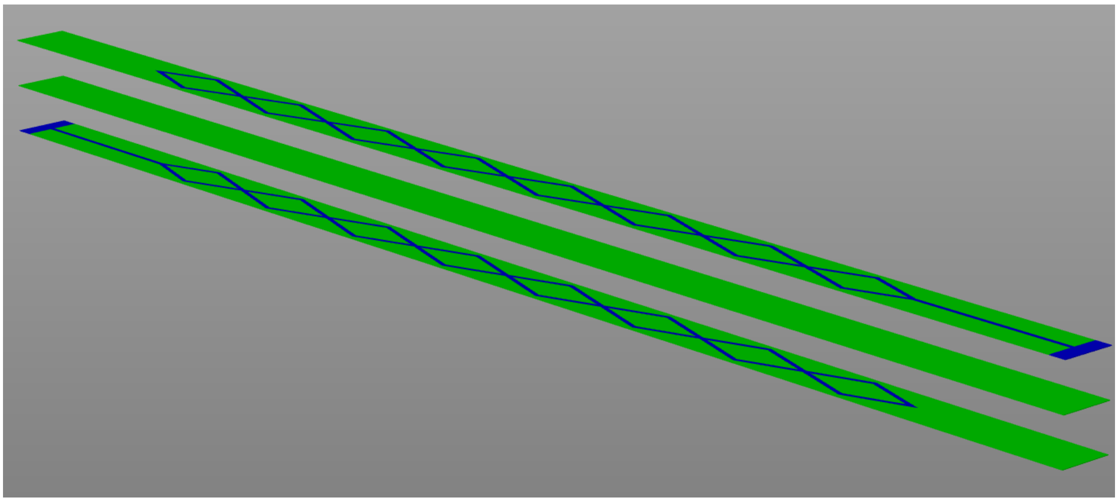

(b)

Figure 3.12: LCS and LTS sensors.

3.4.2 Hysteresis analysis

All the 3D printed sensors were tested in a custom made testing machine to evaluate eventual hysteresis of the sensor. To perform the hysteresis evaluation the sensors were stretched at different percentages of their length until a maximum percentage needed to cover a full flexion of the knee. To asses the amount of the maximum percentage a meter tape was used on a subject's knee. The meter was positioned on the knee fully extended and the initial length of the sensors was chosen as l_0. After the full flexion of the knee the final length l_f was detected, and from the difference between l_f and l_0 the percentage of elongation was extracted using Equation 3.4.

$$Elongation = \frac{l_f - l_0}{l_0} \cdot 100 \tag{3.4}$$

For the 9.50 inches sensors the maximum percentage needed was 20% and 12% for the 11.75 inches. These values of stretching were approximated from the real value needed for covering a full flexion. Integer numbers were chosen to make easier the stretching test. The sensor was fixed in one of its extremity and the other extremity was pulled with a pair of pliers. On each sensor, a line was drawn on the end sections to know precisely the position of the sensor when it was stretched.

All the tests performed on the 3D printed sensors had the aim to evaluate the reliability of the sensors and the eventual hysteresis. For each percentage of stretching the standard deviation was calculated and the hysteresis was calculated as the difference between the same amount of stretching in loading and unloading cycle. In particular, the difference was calculated between the mean value of each percentage of stretching and also between each value. For the longer sensors (LTS and LCS) three samples were printed using the same "Gcode" file. The semi-static and the dynamic tests were performed on each of the three samples as an additional reliability test.

3.4.2.1 Semi-static test

The semi-static test consisted in stretching the sensor starting from l_0 until l_f at steps of 5% for the sensor that needed 20% of stretching and at steps of 3% for the others. In this way, both the 11.75 inches and the 9.50 were stretched at 5 different percentages of their length. The sensors were stretched for a total of 10 cycles, each cycle contains data acquired pulling the sensor (loading cycles) and data during the releasing of the sensor (unloading cycles). A sound chronometer was used to give the sound input on when the sensor has to be stretched, the sensors then were stretched every 3 seconds. Since the data acquired during the travel from a percentage to the next ones weren't in the interest of the test, during the stretching test a videotape was recorded to know precisely when a sensor was at the exact point that needed to be recorded.
The chronometer, the Arduino code, and the video recorder were run at the same time, the sensors were stretched progressively from 0% until 20%/12% and then back to 0%. Thanks to the video only the data acquired during which the sensors

were in the correct position were recorded. The data recorded during the time intervals were then averaged to obtain a single value.

3.4.2.2 Dynamic test

For the dynamic analysis, the sensors were not stretched every 3 seconds and before being stretched to the next percentage the sensors were released to 0%(for example 0% 6% 0% 9% 0%, etc.). Moreover, there were not the time steps since as soon as the sensors had reached the percentage they were released to 0%. For this analysis, only the peak values at the stablished percentages were taken so the averaging process wasn't needed.

3.4.3 Performance validation with the hand goniometer

The same procedure described above for the Adafruit sensor and the Bendlab sensor was used also on one of the 3D printed sensors. In particular, the best sensor in terms of reliability and low hysteresis was chosen for this test. Another factor that was considered for the choice of the best 3D printed sensor was the difficulty of the set up on the soft brace. Also in this case, the sensor was stretched for 10 cycles but from 0 to 90 degrees.

3.4.4 Performance validation with IMUs

A squat test and a gait test were performed on a subject who was wearing both the best 3D printed sensor and the IMUs. Two units were used and set up as described in section 3.3, on the same knee the 3D printed sensor was fixed on a pair of tight pants. Figure 3.13 shows the set up on a right knee of a subject, the 3D printed sensor was fixed with the help of elastic tape, it was also positioned on top of elastic fabric to avoid the direct contact with the pants. The elastic bands used for the IMU were positioned on the top of the tape. The tape is visible on Figure 3.14. Before the test, a calibration process was performed for both IMUs and the 3D printed sensors. For the IMUs only the iSen software was necessary to use, the subject had to stay in a standing position and press the command "Calibration". For the 3D printed sensor instead, the subject was asked to perform 3 squats with increased bending on each squat. The peak values of bending detected by the IMUs and the Arduino board (value in pF) were recorded. In total 4 points were taken (3 bending angles and a zero position) and from them, the calibration line was extracted. After the calibration process, the subject was asked to perform 9 squats, the performance of the 3D printed sensor were evaluated in terms of differences from the IMUs on the peaks of bending. From the differences, the RMSE was calculated with Equation 3.5 where "*f*" (forecast) is the measured

Figure 3.13: 3D printed stretchable sensor and IMUs.

degrees with the 3D printed sensor and "o" (observation) is the value measured by the IMUs.

$$RMSE = \sqrt{(f - o)^2} \tag{3.5}$$

For the gait test, another calibration process was performed, the subject was asked to bend his knee in a standing position, the angles asked were gradually increasing. Also in this test, the points needed for the calibration were 4. For this test, the subject had to walk for 10 steps, rest for 2/3 seconds and then repeat the steps. From this test, a total of 10 peaks were obtained and also in this case the RMSE was calculated on the peaks.

3.4.5 Performance validation with MCS

For the validation of the 3D printed sensor with the MCS system also a squat test and a gait test were performed. The MCS system (provided by stt SYSTEMS San Sebastian,Spain) consisted of 8 cameras fixed all around the room and directed to the center of the room. The “capture” zone was demarcated by red tape, only in that area, the system was able to detect the markers. For detecting the knee motion 4 markers were necessary, all of them positioned on the side of the leg of the subject. More precisely one marker was positioned on the hip, one on the

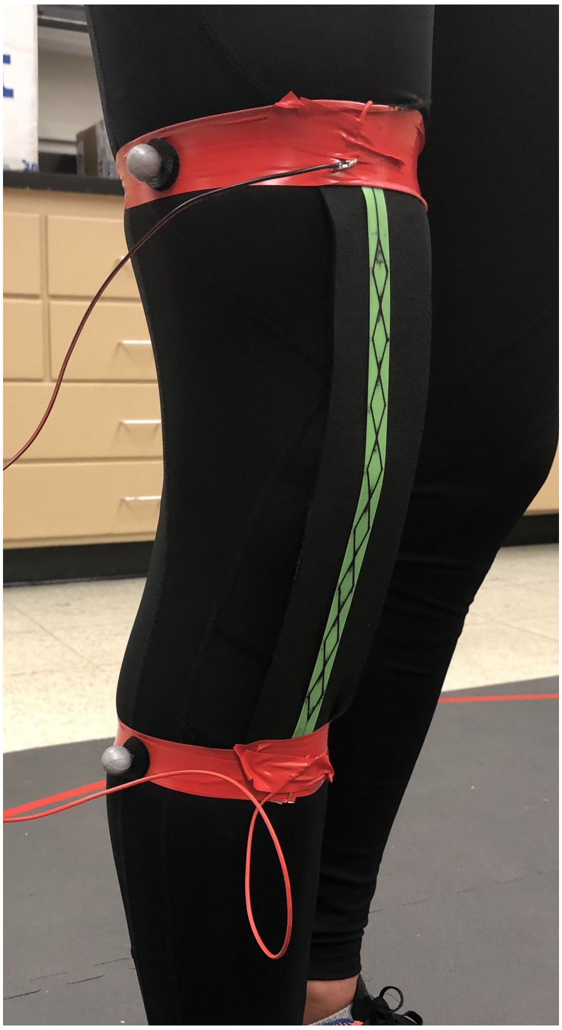

Figure 3.14: 3D printed stretchable sensor and MCS.

distal part of the thigh near the knee, one on the proximal part of the shank also near the knee and one on the ankle. The Squat test was the same described in the section above, also the calibration process was the same. For the gait test instead, the subject performed 48 steps (24 with the sensorized leg) without resting time. The calibration process was the same described for the gait test with the IMU sensors. Figure 3.14 shows the set up with both 3D printed stretchable sensors and the two markers near the knee. During the test, the markers were positioned closer to the knee joint otherwise the system was unable to detect them. For the performance evaluation, the RMSE was calculated for both the tests at the peaks of gait and squat.

Chapter 4

Experimental results

4.1 Flexible sensor

The Adafruit sensor was calibrated using the second-order equations y = $0.0194x^2$ - $13.725x + 2440.4$ ($R^2 = 0.903$). Figure 4.1 shows all the data acquired during the 10 cycles in a graph with the voltage values on the x-axis (the voltage as explained in section 3.1 were rescaled from 0 to 1023) and measured degrees with a hand goniometer on the y-axis. From the graphs is possible to see that with the increasing of the bending angle the voltage values decrease. This behavior is due to an increase of resistance and since it's a voltage divider circuit if one of the two resistance increases the voltage across it decreases.

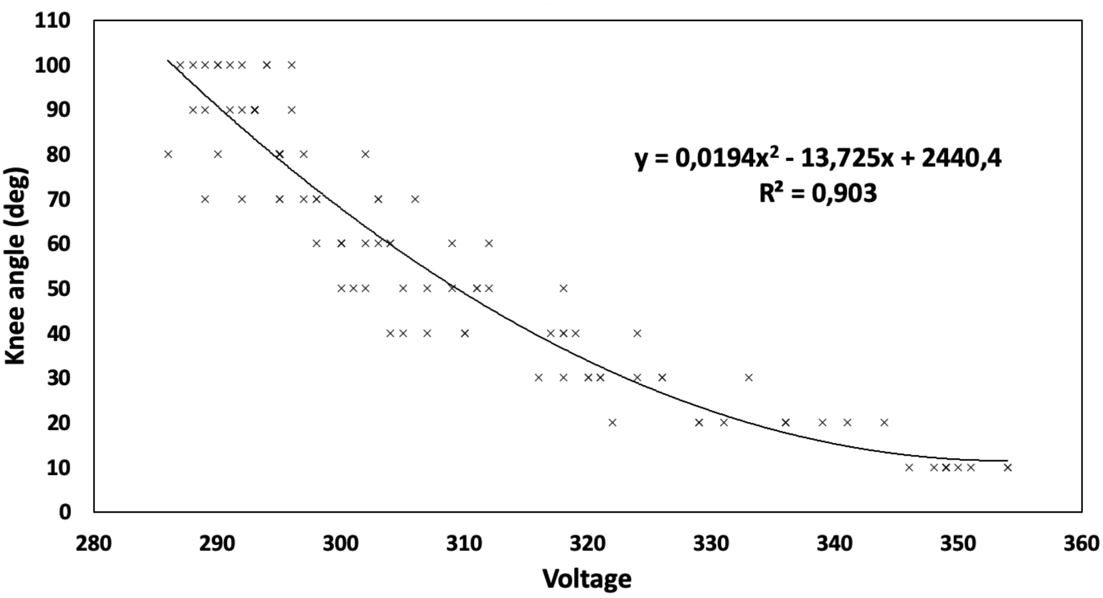

Figure 4.1: Calibration line extracted from data acquired with Arduino UNO board, the voltage values are rescaled following the "Analog pin" mode.

Figure 4.2 shows the data after the transformation in degrees thanks to the

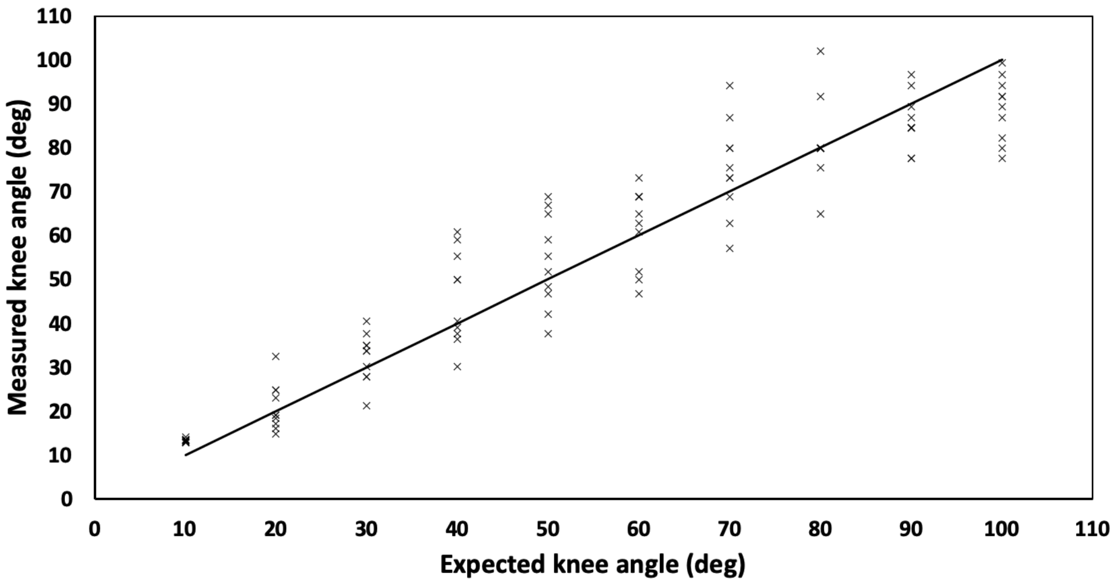

Figure 4.2: Expected knee angle vs measured knee angle by the Adafruit sensor.

calibration line. On the x-axis there are the expected degrees (correct angles measured with the hand goniometer) and on the y-axis there are the measured degrees with the Adafruit sensor. From these graphs is possible to see that the more the sensor is bent the more the performance decrease. Moreover, the "0" angle of bending was not included because no difference was found between the values obtained in "0" degrees of bending and "10". The errors between the measured degrees and the expected degrees are shown in Table 4.1, as stated before the worst performance are present in 100 degrees of bending with error values that reach 22.45 degrees. Also, the absolute mean of the errors (10.87 degrees.) confirms that at 100 degrees of bending the sensor present the worst performance. The lower and the upper limit of accuracy of the sensor, calculated as the max positive and negative difference from the ideal sensor response, were -22.45 and 24.18 degrees. As a percentage of the range the Adafruit sensor presented an accuracy of -22.45% and 24.18%. The RMSE was calculated using equation 3.5 and for this sensor, the value was 9.02 degrees.

4.2 Stretchable sensor

For the Bendlab stretchable sensor, the performance were evaluated before and after the calibration process. Figure 4.3 shows the angle of bending measured with the Bendlab sensor in comparison with the "ideal" sensor line. It's possible to see that the data acquired from the Bendlab App are very far from the "ideal"

Deg	Cyc 1	Cyc 2	Cyc 3	Cyc 4	Cyc 5	Cyc 6	Cyc 7	Cyc 8	Cyc 9	Cyc 10
10	3.02	3.52	3.31	2.88	2.88	3.31	2.88	4.04	3.31	3.15
20	-3.97	4.75	-1.02	-1.69	-5.28	12.42	2.91	-2.91	-1.02	4.75
30	3.67	0.03	-2.20	-2.2	-8.78	10.51	7.66	3.67	4.96	4.96
40	-0.94	-3.71	-2.34	0.51	-9.97	20.87	18.96	15.26	9.99	9.99
50	-3.33	1.71	-1.69	-8.01	-12.34	18.9	16.83	14.81	5.26	8.96
60	-8.29	2.82	0.87	-10.01	-13.33	4.81	13.15	8.90	8.90	8.90
70	16.82	5.33	-7.18	-1.10	-12.91	24.18	9.81	9.81	3.15	3.15
80	21.89	-0.19	-0.19	-0.19	-15.19	11.69	-4.67	-0.19	-0.19	-0.19
90	4.18	-5.55	-5.55	-12.45	-12.45	6.71	-5.55	-5.55	-3.18	-0.76
100	-0.72	-13.18	-17.89	-20.19	-22.45	-3.29	-5.82	-8.31	-10.76	-8.31

Table 4.1: Angles of bending measured with hand goniometer and relative deviations with degrees measured by the Adafruit sensor.

sensor, moreover, the sensor shows really low sensitivity to both minor and major angles of bending. Table 4.2 shows the deviations of the knee angles measured with the Bendlab sensor in comparison with the expected degrees of bending. The Bendlab sensor presented very high deviations in the smaller degrees of bending (0,10,20,30 and 40) and in the higher like 100,110 and 120 degrees, with deviation from 20 to 30 degrees. For this reason, the degrees obtained by the sensor were rescaled using a second-grade equation. The data recorded by the App were plotted as done for the Adafruit sensors. The calibration line was $y = 0.0248x^2 - 1.0244x + 13.442$ with a R^2 of 0.9803 (see Figure 4.4).

Deg	Cyc 1	Cyc 2	Cyc 3	Cyc 4	Cyc 5	Cyc 6	Cyc 7	Cyc 8	Cyc 9	Cyc 10
0	20.1	20.4	21.6	21.8	21.6	20.7	20.6	19.1	19.4	19.7
10	21.9	24.0	19.4	26.3	24.8	30.4	28.4	24.4	22.6	22.4
20	22.8	22.5	19.1	24.9	22.0	28.3	26.8	28.0	21.8	24.0
30	25.4	21.2	22.0	21.2	23.0	22.2	24.9	26.8	22.8	22.3
40	20.0	18.0	19.8	18.5	20.0	18.3	18.2	22.4	20.4	18.3
50	15.0	17.6	17.4	16.8	14.1	13.8	12.4	13.9	14.9	13.9
60	10.4	13.3	9.9	10.0	9.8	9.4	9.4 9	10.1	6.3	6.3
70	6.8	6.4	6.8	4.0	4.9	3.9	2.6	2.8 4	1.8	1.8
80	0.1	-2.1	-1.0	-3.2	-2.9	-4.6	-3.6	-2.8	-2.7	-3.2
90	-6.8	-8.7	-7.3	-10.8	-9.6	-10.9	-10.8	-12.4	-10.6	-11.9
100	-14.2	-16.4	-16.5	-17.2	-17	-16.6	-18.3	-20.6	-19.6	-20.2
110	-21.6	-22.0	-23.6	-23.2	-24.7	-23.8	-26.6	-26.8	-27.2	-27.4
120	-31.5	-30.8	-30	-31.6	-31.2	-29.4	-32.4	-34.4	-35.5	-35.7

Table 4.2: Angles of bending measured with hand goniometer and relative deviations with degrees measured by the Bendlab sensor without the rescaling.

As done for the Adafruit sensor, after the calibration the performance of the sensor were validated in term of accuracy and RMSE. Figure 4.5 shows the data after the rescaling in comparison with the "ideal" sensor response. All the deviations (calculated as difference between the angle measured with the Bendlab

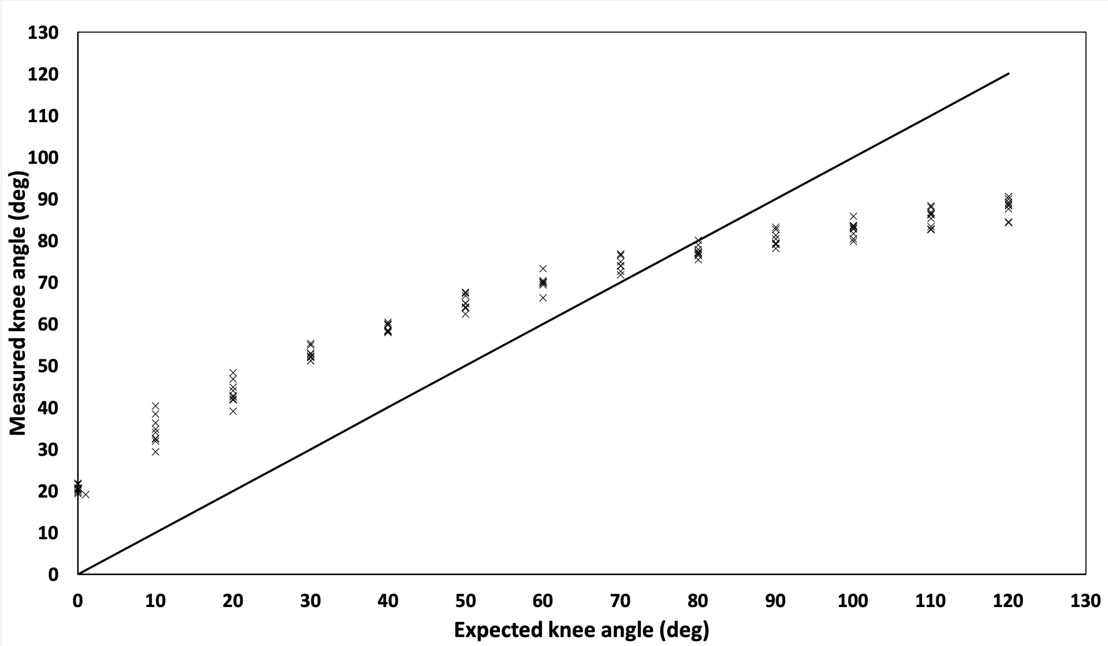

Figure 4.3: Expected degrees vs measured degrees by the Bendlab sensor before the calibration.

sensor and the hand goniometer) acquired during the 10 cycles are shown in Table 4.3, also in this case the worst performance are present in the highest degrees of bending (110 and 120 degrees), however, the Bendlab was able to detect degrees of bending over 100 while the Adafruit sensor wasn't. The upper and the lower limit of accuracy were -16.67 and 11.60 degrees and as a percentage of the range -13.90% and 9.67%. The RMSE of all the data acquired was 5.06 degrees.

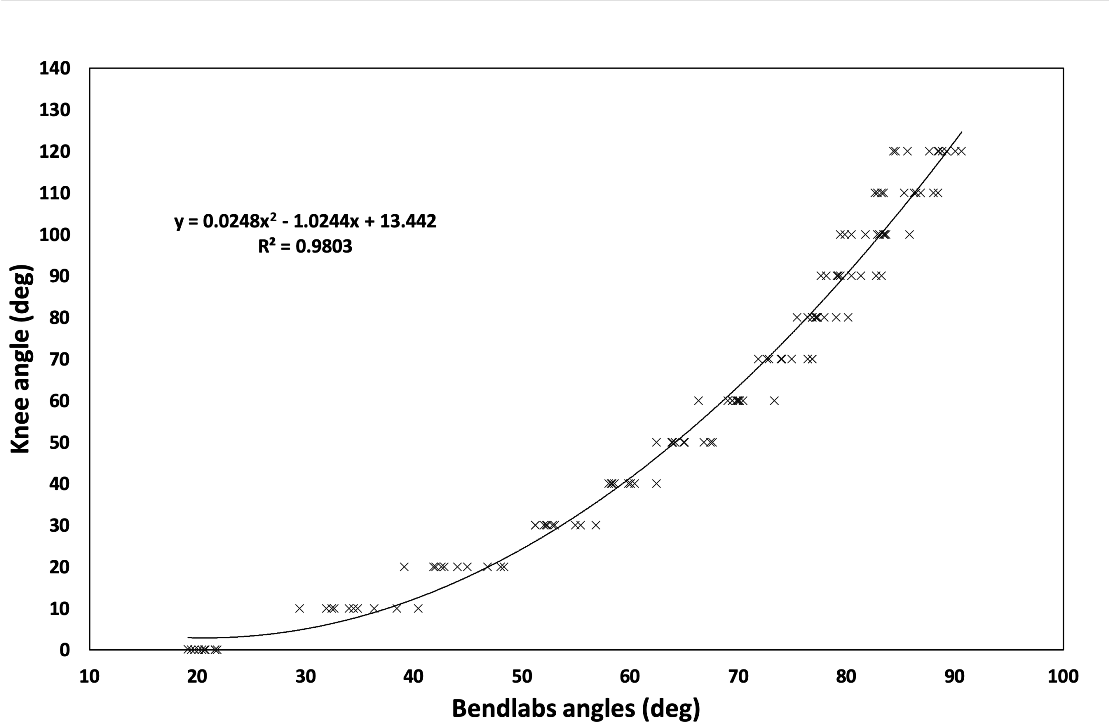

Figure 4.4: Calibration line to rescale Bendlab values. On the x-axis there are the angles detected by the sensor and on the y-axis the angles measured with the hand goniometer.

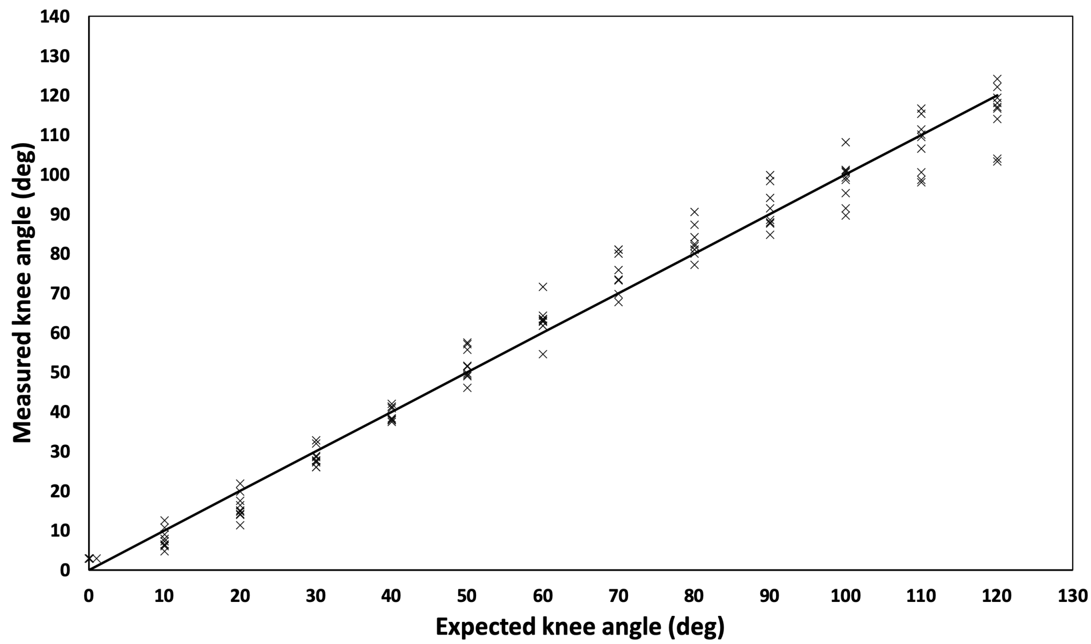

Figure 4.5: Expected knee angle vs measured knee angle by the Bendlab sensor after the calibration.

Deg	Cyc 1	Cyc 2	Cyc 3	Cyc 4	Cyc 5	Cyc 6	Cyc 7	Cyc 8	Cyc 9	Cyc 10
0	2.87	2.87	2.89	2.9	2.89	2.86	2.86	2.92	2.9	2.89
10	-4.00	-2.72	-5.24	-1.07	-2.17	2.53	0.67	-2.45	-3.6	-3.71
20	-4.97	-5.3	-8.7	-2.56	-5.84	1.82	-0.18	1.41	-6.05	-3.62
30	2.81	-4.00	-2.77	-4.00	-1.19	-2.46	1.95	5.27	-1.51	-2.3
40	1.26	-2.55	0.87	-1.61	1.26	-1.99	-2.17	6.08	2.04	-1.99
50	1.64	7.52	7.06	5.68	-0.32	-0.97	-3.92	-0.75	1.42	-0.75
60	4.24	11.6	3.01	3.25	2.77	1.79	1.79	0.83	3.5	-5.46
70	11.04	9.93	11.04	3.44	5.84	3.18	-0.21	0.30	3.44	-2.26
80	10.5	4.14	7.29	1.04	1.88	-2.81	-0.07	2.16	2.44	1.04
90	9.88	4.08	8.34	-2.13	1.39	-2.42	-2.13	-6.71	-1.55	-5.29
100	8.12	1.13	0.82	-1.35	-0.74	0.50	-4.71	-11.55	-8.61	-10.38
110	6.69	5.35	0.06	1.37	-3.49	-0.59	-9.50	-10.12	-11.35	-11.97
120	-2.98	-0.61	2.13	-3.31	-1.97	4.20	-5.99	-12.53	-16.04	-16.67

Table 4.3: Angles of bending measured with hand goniometer and relative deviations with degrees measured by the Bendlab sensor after the calibration.

4.3 IMUs

For the IMUs analysis, only the comparison with the hand goniometer was done and the results are shown in Figure 4.6. The calibration process as performed for the other sensors wasn't needed, the IMUs indeed presented a support Software that allows the user to perform a calibration process before using them. All the deviations (calculated as the difference from the measured angle with the IMU and the hand goniometer) during the 10 cycles are shown in Table 4.4. In this case, there are not precise degrees of bending that causes errors, indeed also for higher degrees of bending the performance of the IMUs are really close to the hand goniometer. The lower and the upper limit of accuracy were -4.7 and 3.8 degrees and -3.9%, 3.1% respect to the range of degrees measured. These results find confirmation also in the RMSE with a value of 1.91 degrees which is lower than the RMSE found for the Adafruit and the Bendlab sensors. Another advantage of these sensors is that the calibration process is really fast, indeed the subjects had only to stay in a stand position for less than 2 seconds (in the meantime the "calibration" command on the software has to be pressed) and the sensors are calibrated.

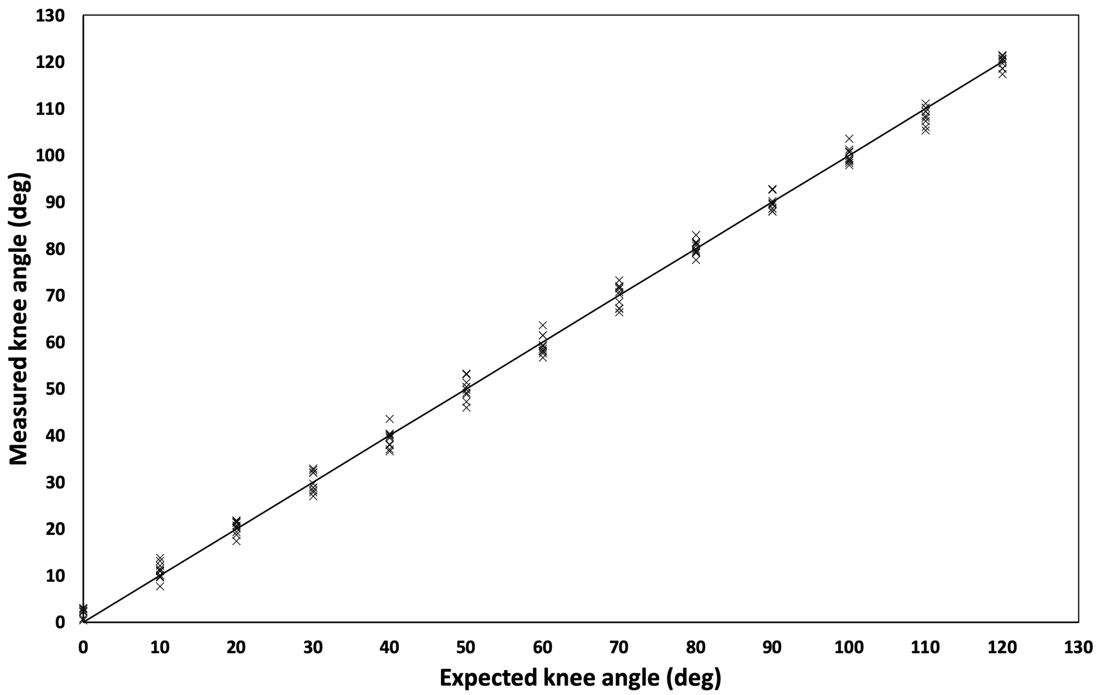

Figure 4.6: Expected knee angle vs measured knee angle by IMUs.

Deg	Cyc 1	Cyc 2	Cyc 3	Cyc 4	Cyc 5	Cyc 6	Cyc 7	Cyc 8	Cyc 9	Cyc 10
0	0.7	2.4	2.8	2.2	3.1	0.7	0.4	2.7	2.2	2.2
10	0.1	0.9	1.1	-0.4	3.8	2.1	3.1	1.4	-0.2	-2.3
20	0.1	1.8	-0.7	0.7	-2.6	1.3	0.4	1.6	1.4	-1.3
30	-0.3	-1.2	-1.2	2.1	-1.8	2.9	2.6	2.0	-3.0	-2.2
40	-3.0	-0.2	-1.9	0.1	-0.6	0.4	0.4	3.5	-2.1	-3.4
50	3.1	3.2	-2.8	-0.2	-4.0	-1.2	0.4	1.3	-0.9	0.4
60	1.4	1.4	3.6	-2.0	-0.9	-0.7	-1.8	-1.4	-2.4	-3.3
70	0.2	1.5	3.2	-2.8	-2.9	2.0	1.8	-1.4	0.7	-3.6
80	1.4	2.9	1.2	1.1	-2.4	-0.2	-0.5	-0.9	0.7	-0.8
90	-2.0	2.6	-0.3	-0.6	2.8	-1.4	-1.4	0.2	-0.2	-2.1
100	-0.7	0.8	3.6	0.6	-1.2	-2.1	-0.7	1.2	-1.6	-1.0
110	-2.0	0.2	0.2	-2.7	1.1	-1.6	-0.7	-0.6	-3.9	-4.7
120	1.2	0.3	-0.3	0.6	0.7	-1.5	0.7	1.5	-2.6	-1.4

Table 4.4: Angles of bending measured with hand goniometer and relative deviations with degrees measured by the IMUs.

4.4 3D printed stretchable sensors

As described in section 3.3 before performing the performance analysis with the hand goniometer, different tests were done on different models of the 3D printed stretchable sensor in order to choose which one was the best for measuring knee motions. In this section, the stretchable properties and performance of the RS, the SCS, the LCS, and the LTS are shown.

4.4.1 Hysteresis evaluation

4.4.1.1 RS sensor semi-static test

Table 4.5 and Figure 4.7 shows all the resistance values acquired during the 10 cycles of the semi-static stretching test. Since the length of the sensor was 9.5 inches the percentage needed to cover a full flexion of the knee was 20%. On the left side of the table is possible to see all the percentages of stretching increasing before reaching the max percentage and then decreasing. In this way is possible to evaluate the hysteresis of the sensor (calculated as described in section 3.4.2). Figure 4.8 shows all the data acquired during the semi-static test. Figure 4.9 shows the mean values in the loading and unloading cycles. From this graph is possible to see that the values of resistance of the RS ,when it passes from loading to the unloading cycle, keep staying lower than the loading cycles. The hysteresis absolute values are similar in the 5%,10% and 15% with 21.99, 21.68 and 21.57 $k\Omega$. The higher value of standard deviation was found in 0% of stretching and in 5% of stretching during the unloading cycles with values of 15.94 and 13.74 $k\Omega$. If evaluated in percentages of the range of values the hysteresis was 5.00%, 4.92% and 4.90% for 5, 10 and 15% of stretching.

%	Cyc 1	Cyc 2	Cyc 3	Cyc 4	Cyc 5	Cyc 6	Cyc 7	Cyc 8	Cyc 9	Cyc 10
0	575.58	624.43	613.28	620.09	600.93	602.30	601.38	593.93	586.83	582.84
5	313.68	297.32	294.54	298.48	311.87	300.14	306.17	311.60	313.67	303.66
10	235.05	226.36	228.18	224.57	222.91	225.28	223.45	221.25	226.15	221.76
15	220.64	211.04	208.08	207.32	207.12	210.70	206.80	206.68	205.93	206.24
20	221.31	211.89	208.08	207.41	207.82	206.77	205.90	206.60	204.94	205.65
15	192.55	187.37	187.55	187.87	188.71	187.81	185.74	185.74	187.04	184.40
10	209.01	201.60	201.10	207.68	202.66	206.23	206.23	203.12	199.59	201.01
5	258.83	290.33	299.03	278.46	298.33	300.43	277.98	279.92	269.08	278.78

Table 4.5: Resistance values of RS in $k\Omega$ at different percentages of stretching in the semi-static test.

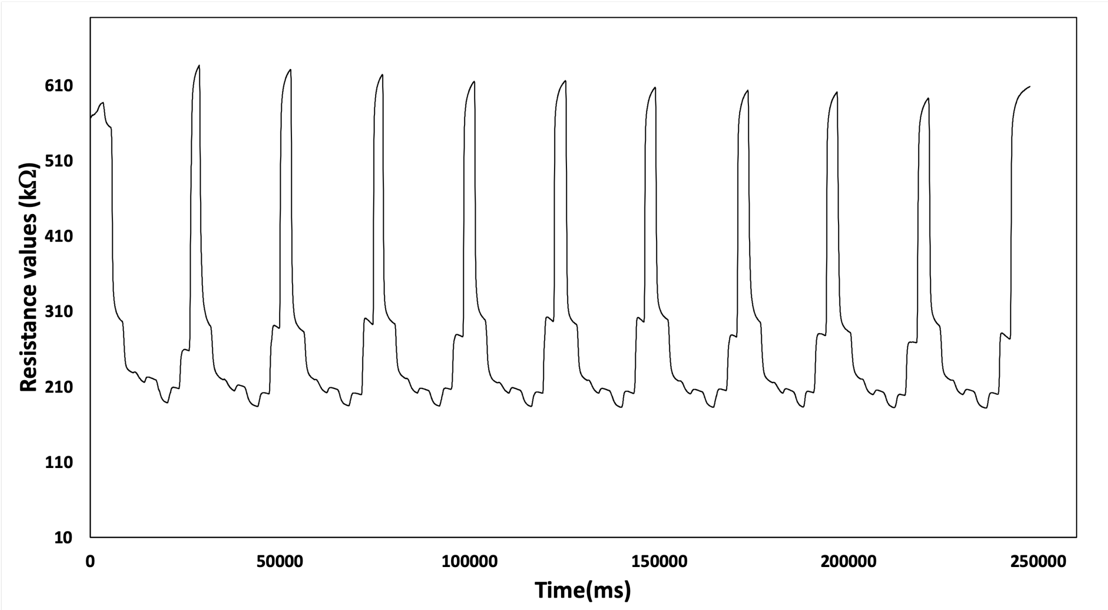

Figure 4.7: Data acquired from the RS in the semi-static test.

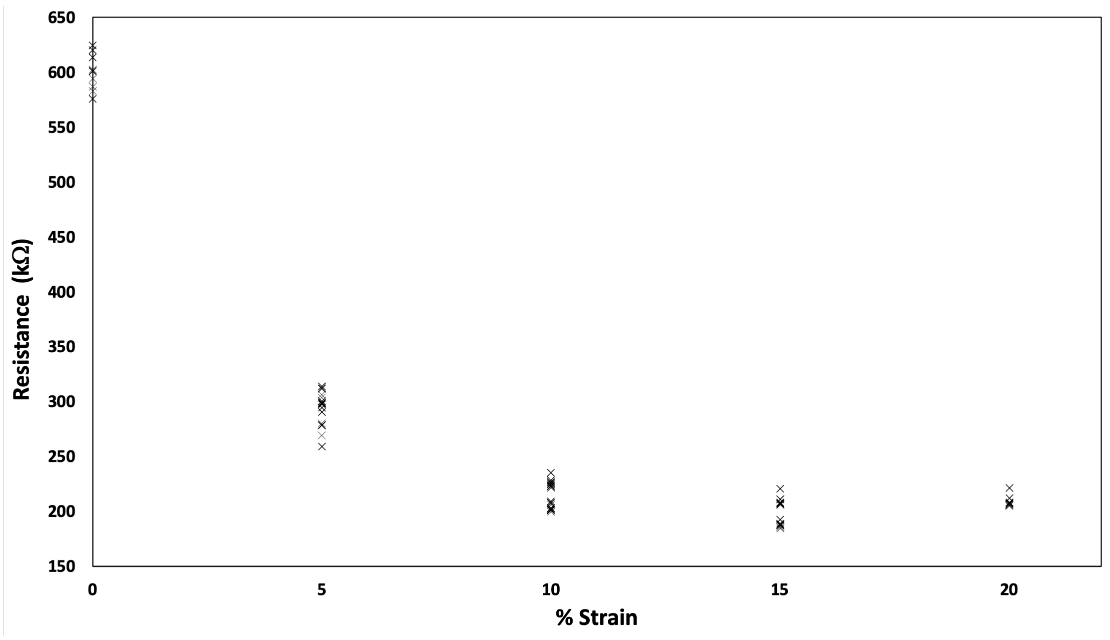

Figure 4.8: Data acquired from the RS at different percentages of stretching in the semi-static test.

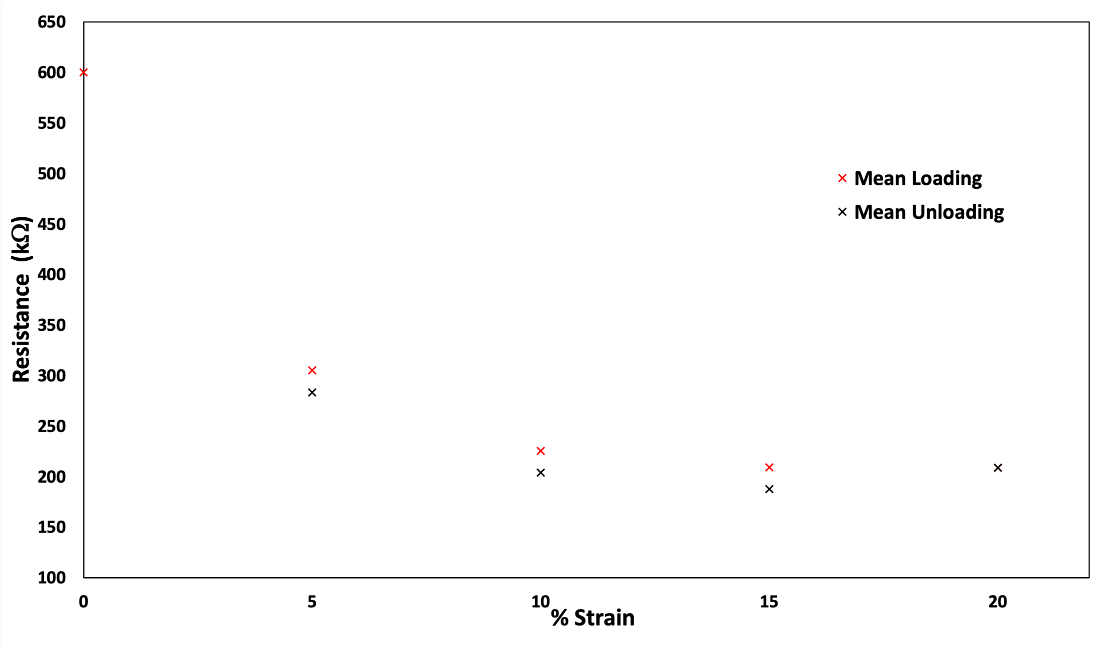

Figure 4.9: Mean of loading and unloading cycles acquired from RS at different percentages of stretching in the semi-static test.

4.4.1.2 SCS sensor semi-static test

Table 4.6 and Figure 4.10 shows all the capacitance values acquired during the 10 cycles of the semi-static stretching test. Since the length of the sensor was 9.5 inches the percentage needed to cover a full flexion of the knee was 20%. Figure 4.11 shows all the data acquired during the semi-static test. Figure 4.12 shows the mean values in the loading and unloading cycles. From this graph is possible to see that the SCS when it passes from loading to the unloading cycle the values of capacitance keep staying higher than the loading cycles. The hysteresis absolute values are increasing with the percentage of stretching with 24.67, 53.97 and 85.66 pF for 5%,10%, and 15%. The higher value of standard deviation was found in 15% of stretching during the unloading cycles with a value of 30.63 pF and in 15% during the loading cycles with a value of 24.79 pF. If evaluated as a percentage of the range of values the hysteresis was 7.88%, 17.23% and 27.36% for 5, 10 and 15% of stretching.

%	Cyc 1	Cyc 2	Cyc 3	Cyc 4	Cyc 5	Cyc 6	Cyc 7	Cyc 8	Cyc 9	Cyc 10
0	33.01	40.62	42.26	45.63	41.87	43.93	43.22	43.36	44.58	43.19
5	65.04	67.56	85.6	75.46	83.33	88.07	78.00	78.22	78.45	83.41
10	128.50	149.11	164.08	168.76	156.68	164.38	174.24	183.58	177.87	181.47
15	171.17	187.25	208.49	238.18	225.10	225.06	221.16	222.23	254.33	239.51
20	178.43	203.74	212.19	235.63	223.32	238.38	214.77	255.4	242 .00	242.38
15	240.58	282.75	284.62	329.72	307.36	346.12	314.02	325.46	325.69	292.79
10	193.14	196.60	222.01	233.46	245.47	218.57	209.89	236.72	224.66	207.75
5	112.10	101.89	109.62	116.55	105.40	84.44	96.39	97.54	99.17	106.72

Table 4.6: Capacitance values of SCS in pF at different percentages of stretching.

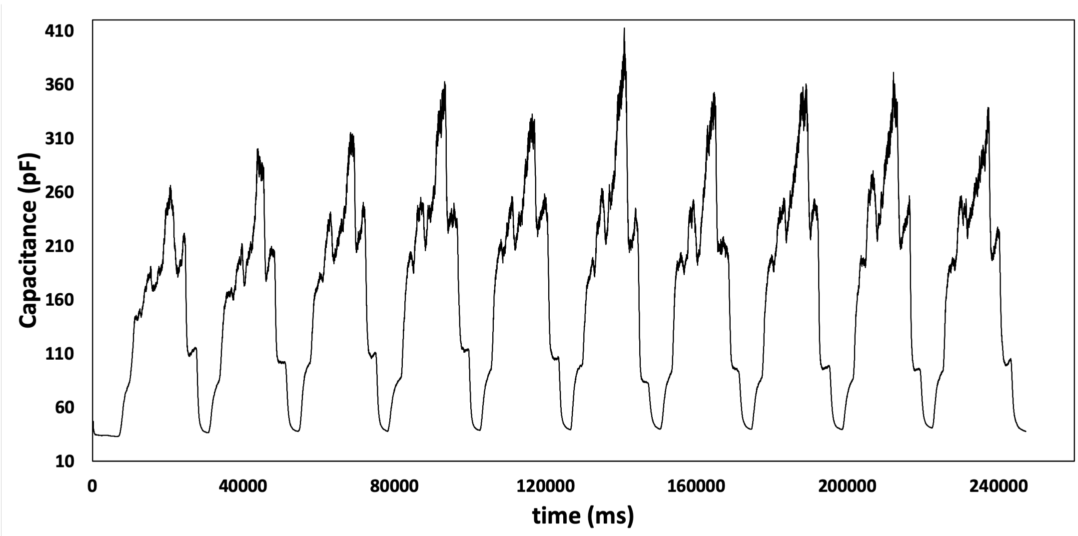

Figure 4.10: Data acquired from the SCS in the semi-static test.

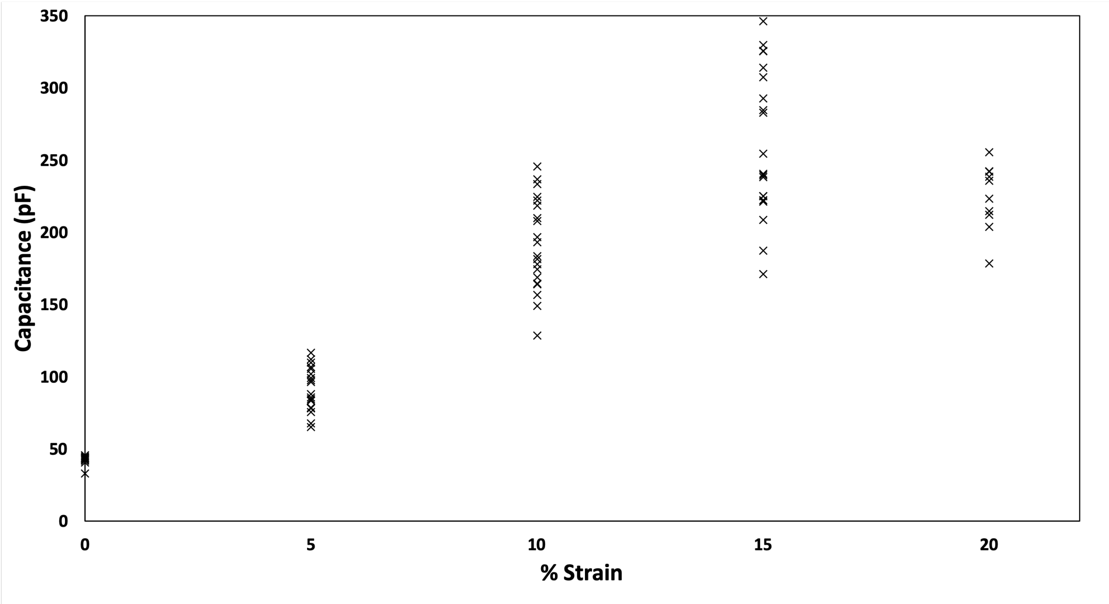

Figure 4.11: Data acquired from the SCS at different percentages of stretching in the semi-static test.

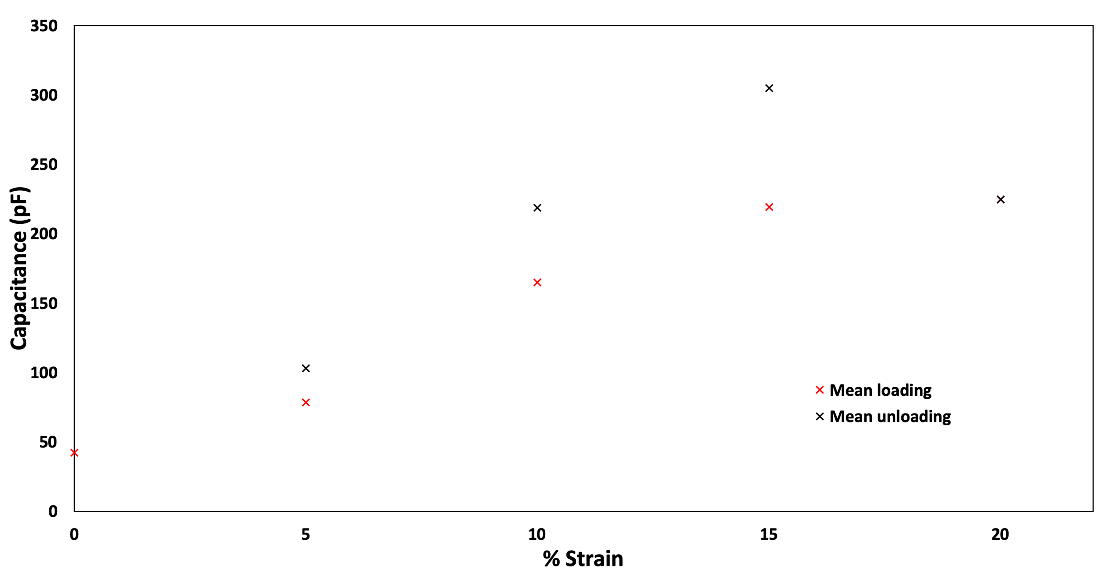

Figure 4.12: Mean of loading and unloading cycles acquired from SCS at different percentages of stretching in the semi-static test.

4.4.1.3 LCS sensor semi-static test

Table 4.7 and Figure 4.13 shows all the capacitance values acquired during the 10 cycles of the semi-static stretching test. Since the length of the sensor was 11.75 inches the percentage needed to cover a full flexion of the knee was 12%. Figure 4.14 shows all the data acquired during the semi-static test. Figure 4.15 shows the mean values in the loading and unloading cycles. From this graph is possible to see that the LCS when it passes from loading to the unloading cycle the values of capacitance keep staying higher than the loading cycles. The hysteresis absolute values are 0.80, 2.53 and 2.30 pF for 3%, 6%, and 9%. The higher value of standard deviation was found in 3% of stretching during the loading cycles with a value of 1.63 pF and in 3% during the unloading cycles with a value of 1.05 pF. If evaluated in percentages of the range of values the hysteresis was 2.86%, 9.01% and 8.20% for 3, 6 and 9% of stretching.
For this sensor 3 samples from the same "Gcode" file were printed to test the reliability of the sensor in the stretching test. Figure 4.16 shows the behavior of the three sensors tested and shows that, even if the values are not the same for each sample, they have very similar patterns in response to the stretching. Also, the results related to the hysteresis and the standard deviation are similar, in particular, the other two sensors presented 0.3, 2.07, 2.78 pF and 1.29, 3.39 and 3.47 pF of hysteresis for 3%, 6% and 9% of stretching. In percentage of the range the hysteresis values are 1.08%, 7.41%, 9.96% and 3.96%, 10.41%, 10.66%. For one sample the higher values of standard deviation were 1.19 and 1.52 pF in the 3% of stretching during the loading and unloading cycles (like the first LCS tested), for the other sample were 1.16 pF at 9% in the unloading cycles and 1.15 pF at 6% in the unloading cycles.

%	Cyc 1	Cyc 2	Cyc 3	Cyc 4	Cyc 5	Cyc 6	Cyc 7	Cyc 8	Cyc 9	Cyc 10
0	32.50	33.66	33.79	34.36	34.25	34.33	34.35	35.16	35.17	35.28
3	39.17	42.40	41.67	44.15	44.18	43.21	43.62	44.71	44.00	43.31
6	50.63	51.63	50.67	52.10	52.26	52.48	52.41	53.25	52.63	53.49
9	55.66	56.38	56.08	56.54	56.89	57.04	57.27	58.34	57.96	58.47
12	57.79	58.37	57.96	59.18	58.98	59.68	59.60	60.19	60.34	60.08
9	58.31	58.40	58.95	59.24	59.22	59.36	59.44	60.14	60.04	60.55
6	54.12	54.25	54.28	54.36	54.75	54.74	54.41	55.16	55.52	55.22
3	44.36	43.35	43.10	41.89	43.86	43.10	43.59	45.07	45.10	44.99

Table 4.7: Capacitance values in pF of LCS at different percentages of stretching in the semi-static test.

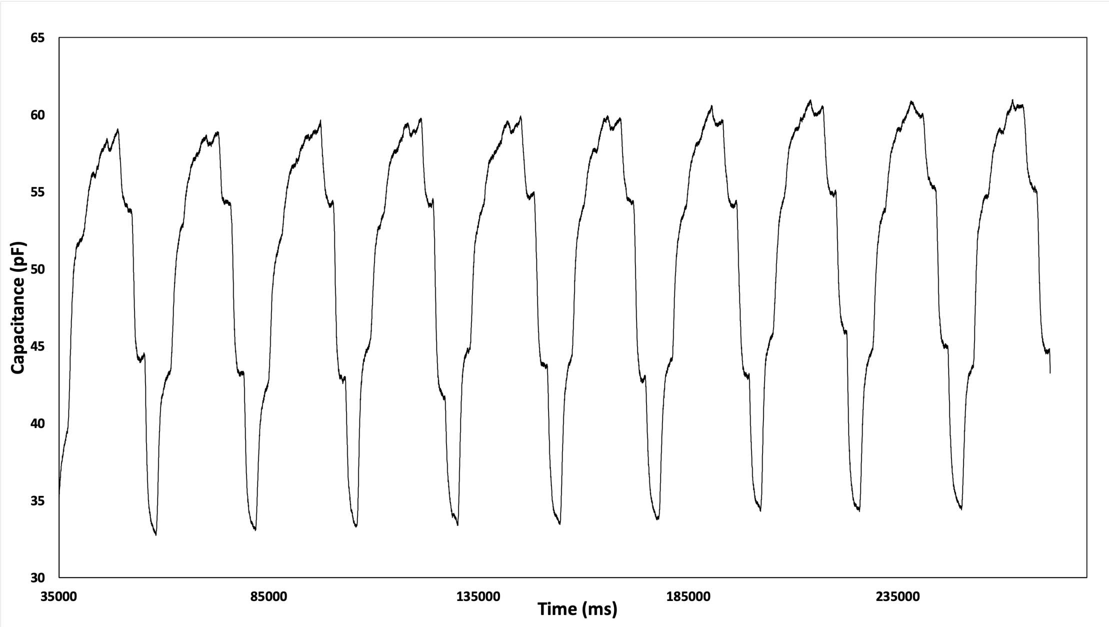

Figure 4.13: Data acquired from the LCS in the semi-static test.

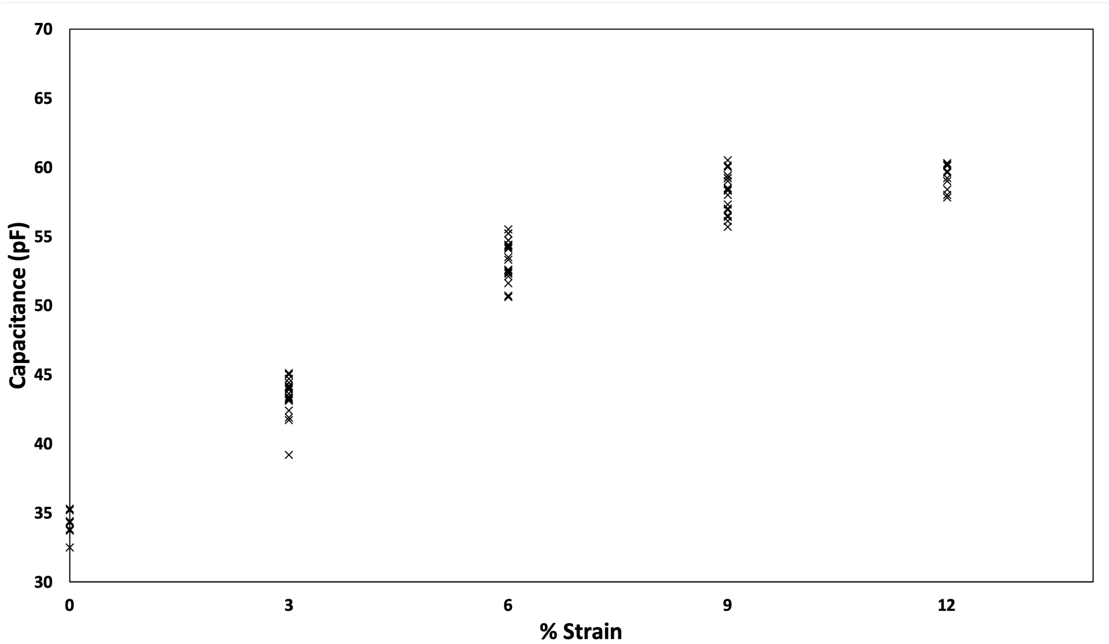

Figure 4.14: Data acquired from the LCS at different percentages of stretching in the semi-static test.

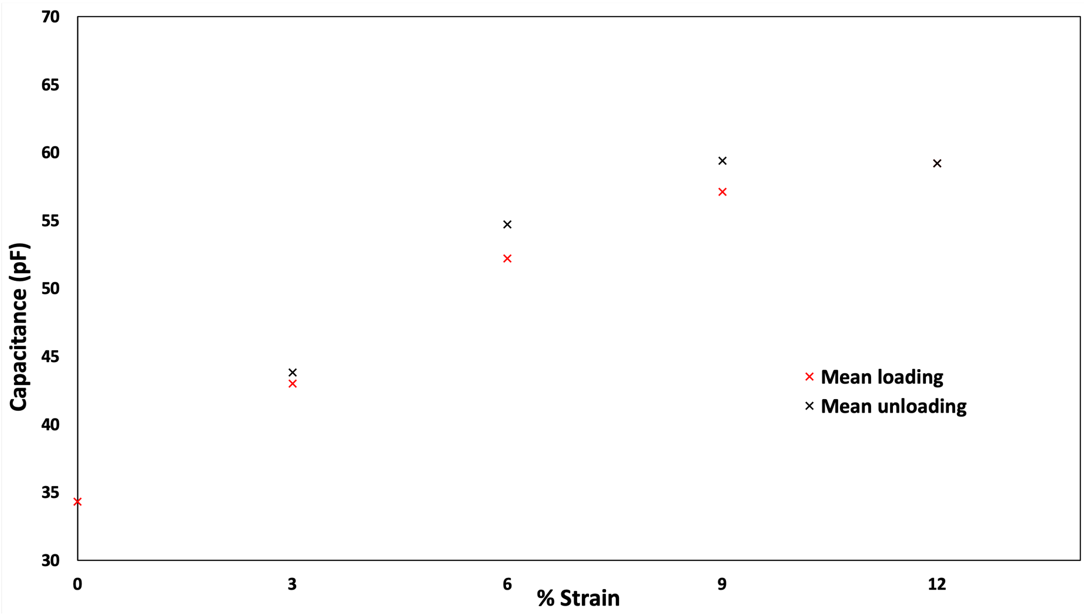

Figure 4.15: Mean of loading and unloading cycles acquired from LCS at different percentages of stretching in the semi-static test.

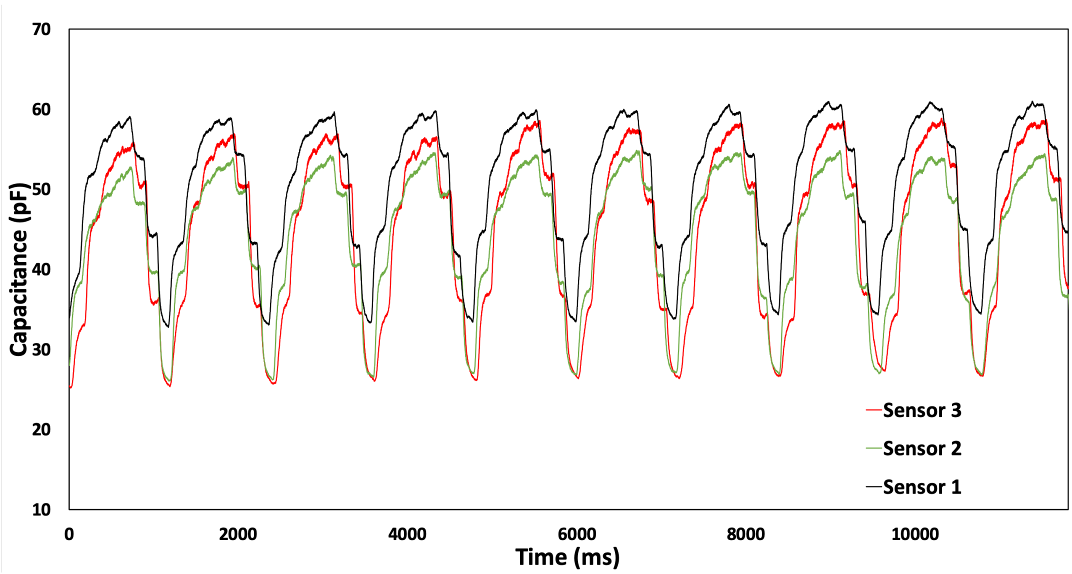

Figure 4.16: Semi-static stretching test with 3 samples of LCS.

4.4.1.4 LTS sensor semi-static test

Table 4.8 and Figure 4.17 shows all the capacitance values acquired during the 10 cycles of the semi-static stretching test. Since the length of the sensor was 11.75 inches the percentage needed to cover a full flexion of the knee was 12%. Figure 4.18 shows all the data acquired during the semi-static test. Figure 4.19 shows the mean values in the loading and unloading cycles. From this graph is possible to see that the LTS when it passes from loading to the unloading cycle the values of capacitance keep staying higher than the loading cycles. The hysteresis absolute values are 1.07,5.90 and 8.39 pF for 3%, 6%, and 9%. The higher value of standard deviation was found in 9% of stretching during the unloading cycles with a value of 2.65 pF and in 12% with a value of 2.52 pF. If evaluated as a percentage of the range of values the hysteresis was 2.00%, 10.98% and 15.62% for 3, 6 and 9% of stretching.
For this sensor also 3 samples from the same "Gcode" file were printed to test the reliability of the sensor in the stretching test. Figure 4.20 shows the behavior of the three sensors tested and shows that, even if the values are not the same for each sample, they have very similar patterns in response to the stretching. In particular, one sensor presented higher values than the other two, but also in this case, the pattern is similar. Also the results related to the hysteresis and the standard deviation are similar, in particular, the other two sensors presented 0.78, 4.78, 6.36 pF and 1.14, 4.08 and 6.48 pF of hysteresis for 3%, 6% and 9% of stretching. In percentage of the range the hysteresis values are 2.01%, 12.34%, 16.42% and 3.07%, 10.94%, 17.38%. For one sample the higher values of standard deviation were 1.97 pF for both the 9% of stretching during the loading and unloading cycles, for the other sample were 2.40 pF at 9% in the unloading cycles and 2.21 pF at 6% in the unloading cycles.

%	Cyc 1	Cyc 2	Cyc 3	Cyc 4	Cyc 5	Cyc 6	Cyc 7	Cyc 8	Cyc 9	Cyc 10
0	16.1	16.6	17.01	17.29	17.91	17.9	18.11	18.56	18.41	18.29
3	30.46	31.78	31.19	31.84	31.64	30.69	32.10	31.44	31.28	29.77
6	45.44	47.68	47.46	49.30	50.11	50.00	51.34	50.17	50.41	50.53
9	54.48	56.57	56.47	58.20	58.23	59.58	60.64	60.41	60.43	60.68
12	56.78	59.26	60.49	61.70	61.68	63.05	63.48	64.86	63.76	64.28
9	61.88	64.12	64.71	66.26	67.63	68.64	68.23	69.81	68.51	69.82
6	51.44	55.35	54.54	53.83	54.77	55.25	54.51	58.49	55.71	57.58
3	31.39	34.09	33.82	33.11	34.15	32.42	27.37	32.42	31.39	32.77

Table 4.8: Capacitance values in pF of LTS at different percentages of stretching in the semi-static test.

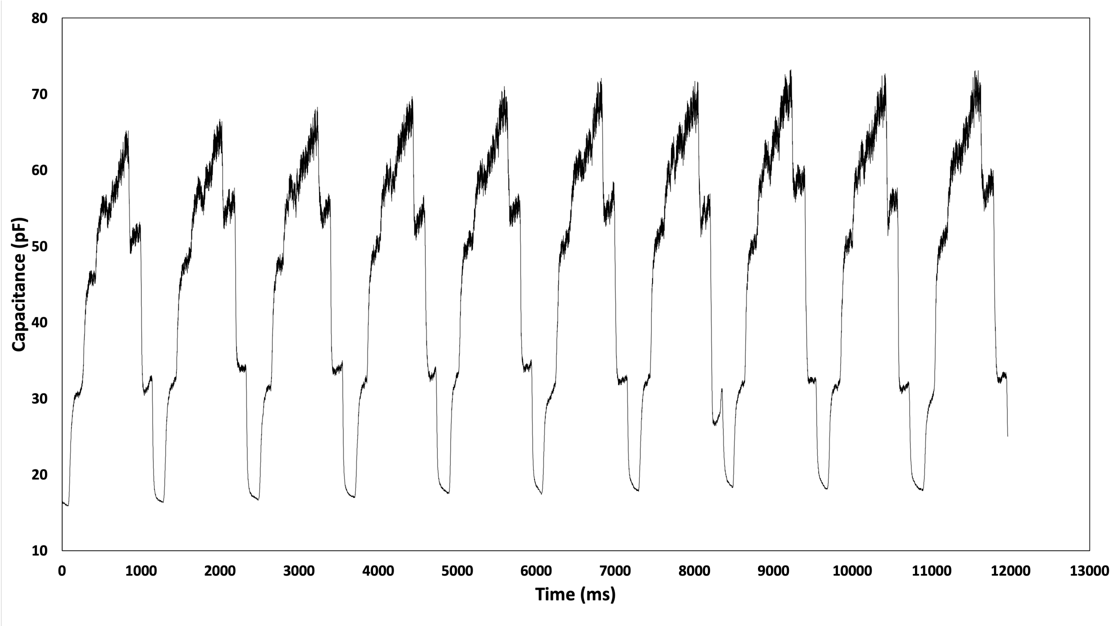

Figure 4.17: Data acquired from the LTS in the semi-static test.

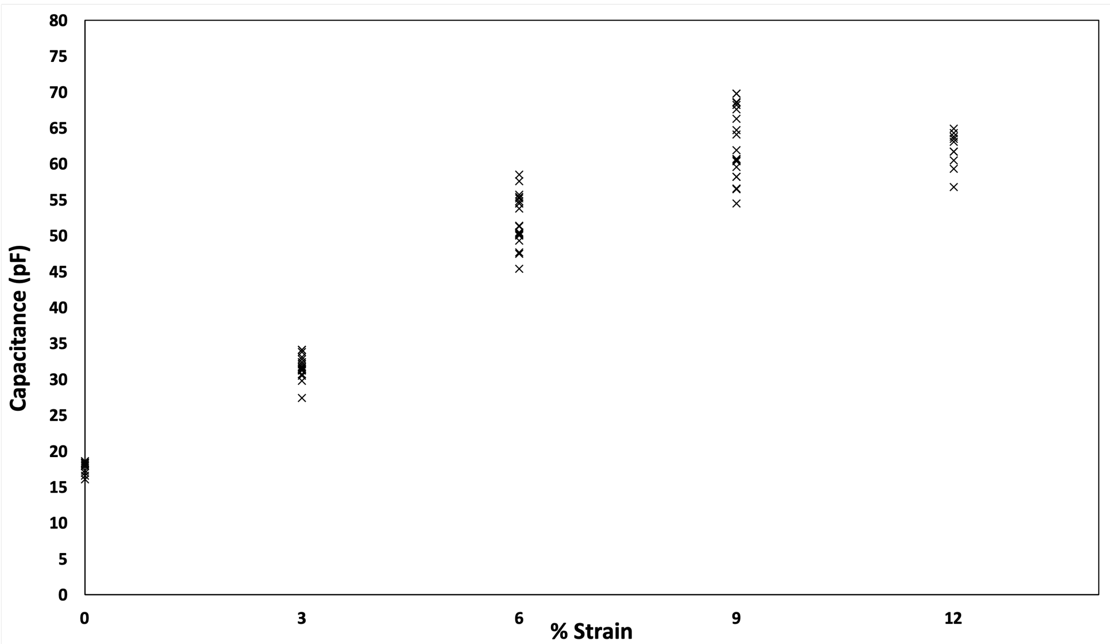

Figure 4.18: Data acquired from the LTS at different percentages of stretching in the semi-static test.

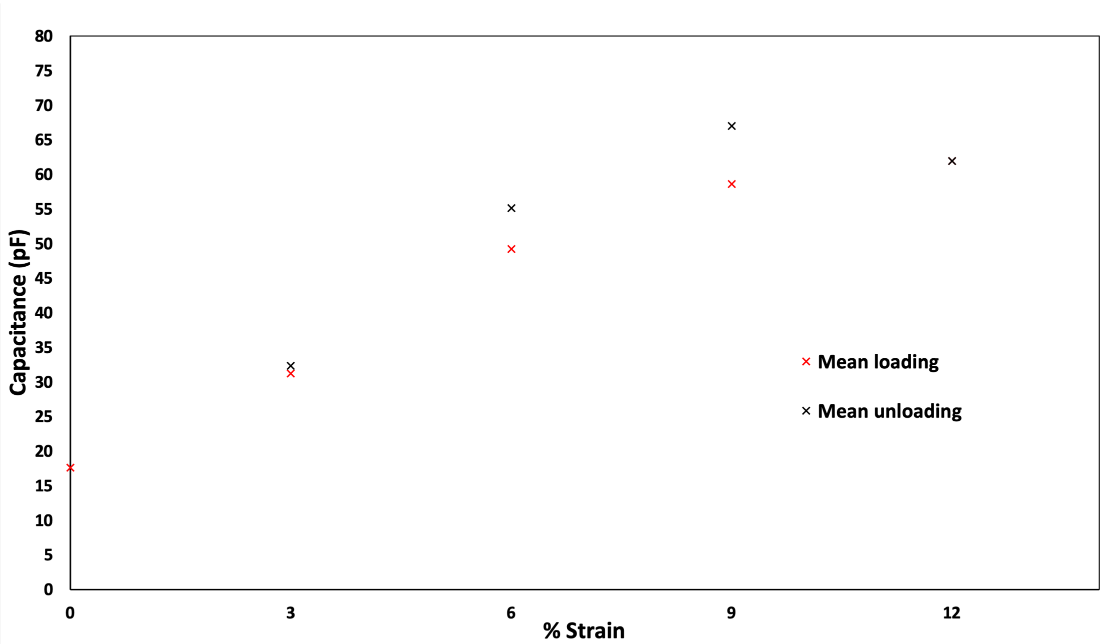

Figure 4.19: Mean of loading and unloading cycles acquired from LTS at different percentages of stretching in the semi-static test.

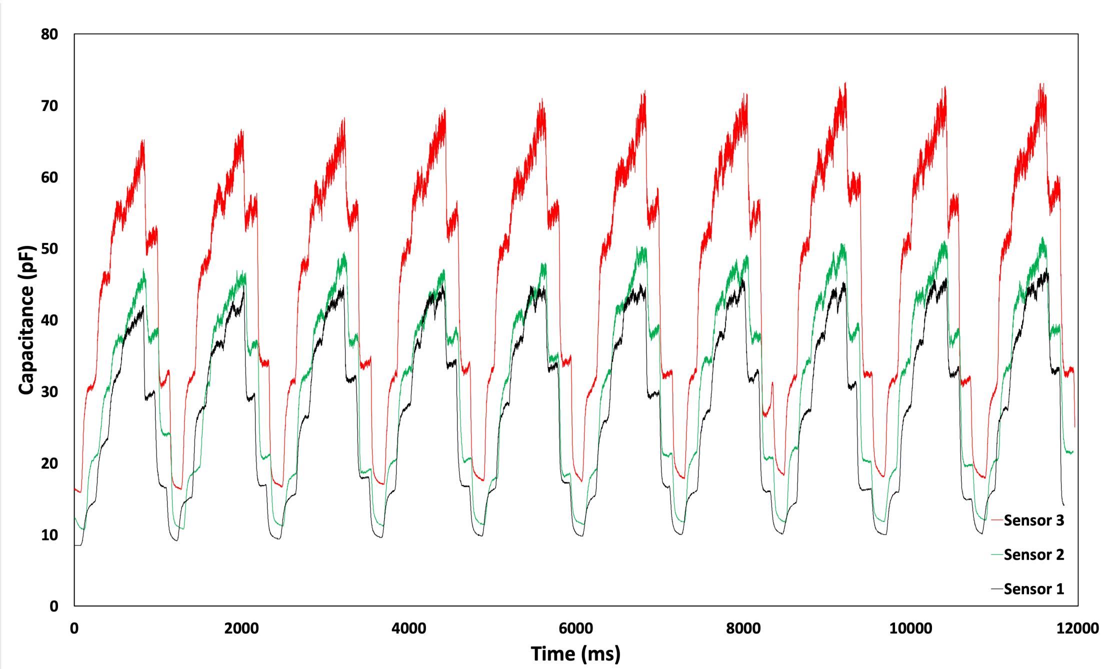

Figure 4.20: Semi-static stretching test with 3 samples of LTS in the semi-static test.

4.4.1.5 LCS sensor dynamic test

Table 4.9 and Figure 4.21 shows all the capacitance values acquired during the 10 cycles of the dynamic stretching test. Figure 4.22 shows all the data acquired during the semi-static test, It is possible to see how the sensor behaves in response to a faster stretching than the one tested in the semi-static test. Figure 4.23 shows the mean values in the loading and unloading cycles. From this graph is possible to see that the LCS sensor presents less hysteresis than the semi-static test. Indeed the hysteresis absolute values are 0.29, 0.19 and 0.21 pF for 3%, 6% and 9%. The higher value of standard deviation was found in 6% of stretching during the loading cycles with a value of 2.40 pF and in 9% in the loading cycles with a value of 2.31 pF. If evaluated as a percentage of the range of values the hysteresis was 1.07%, 0.71% and 0.79% for 3, 6 and 9% of stretching.
For this sensor also 3 samples from the same "Gcode" file were printed in order to test the reliability of the sensor in the dynamic stretching test. The results related to the hysteresis and the standard deviation are similar, in particular, the other two sensors presented 1.21, 3.29 and 2.2 pF and 0.15, 0.66 and 0.36 pF of hysteresis for 3%, 6% and 9% of stretching. In percentage of the range the hysteresis values are 4.28%, 11.61%, 7.78% and 0.56%, 2.48%, 1.36%. For one sample the higher values of standard deviation were 2.59 pF for the 6% of stretching during the unloading cycles and 2.10 pF for 9% during the loading cycles, for the other sample were 1.72 pF at 9% in the unloading cycles and 1.25 pF at 6% in the unloading cycles.

%	Cyc 1	Cyc 2	Cyc 3	Cyc 4	Cyc 5	Cyc 6	Cyc 7	Cyc 8	Cyc 9	Cyc 10
0	35.92	34.73	38.28	36.53	37.74	37.65	37.13	37.20	37.54	37.92
3	44.44	51.94	48.14	44.39	46.30	46.66	47.09	46.74	46.86	43.92
6	50.23	57.61	53.73	53.37	53.02	52.57	53.38	54.67	55.52	58.30
9	54.98	57.81	58.38	58.24	59.20	58.74	58.96	59.73	58.52	61.52
12	58.84	58.19	61.11	61.03	61.35	58.14	60.86	60.39	60.32	61.52
9	57.92	58.19	59.00	57.71	58.35	58.14	59.17	58.98	57.90	58.60
6	54.02	55.22	54.13	53.89	52.48	52.75	54.76	54.70	54.59	53.98
3	46.2	47.76	45.64	48.65	47.57	46.69	45.25	47.04	46.21	48.34

Table 4.9: Capacitance values in pF of LCS at different percentages of stretching in the dynamic test.

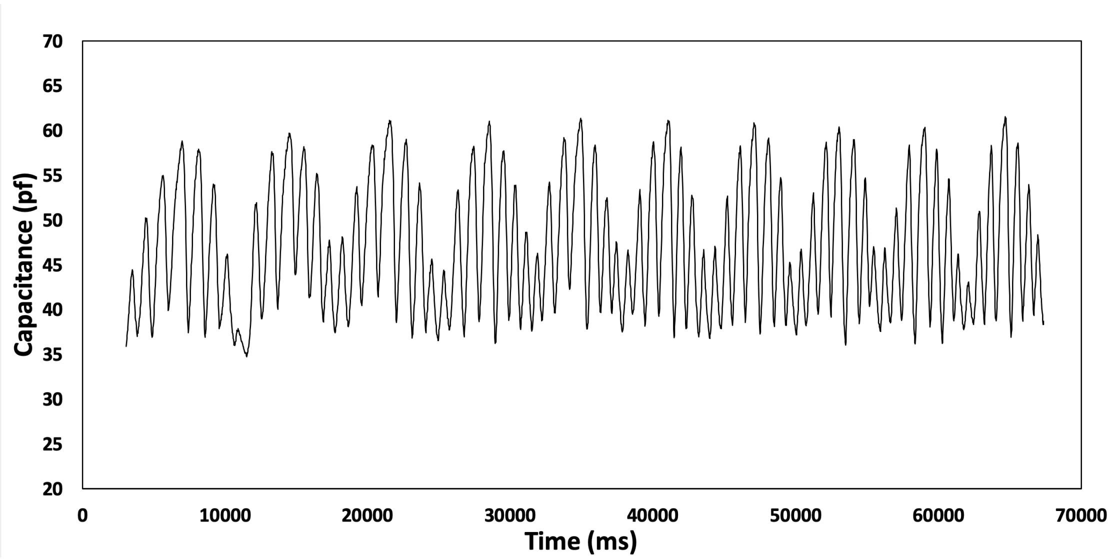

Figure 4.21: Data acquired from the LCS in the dynamic test.

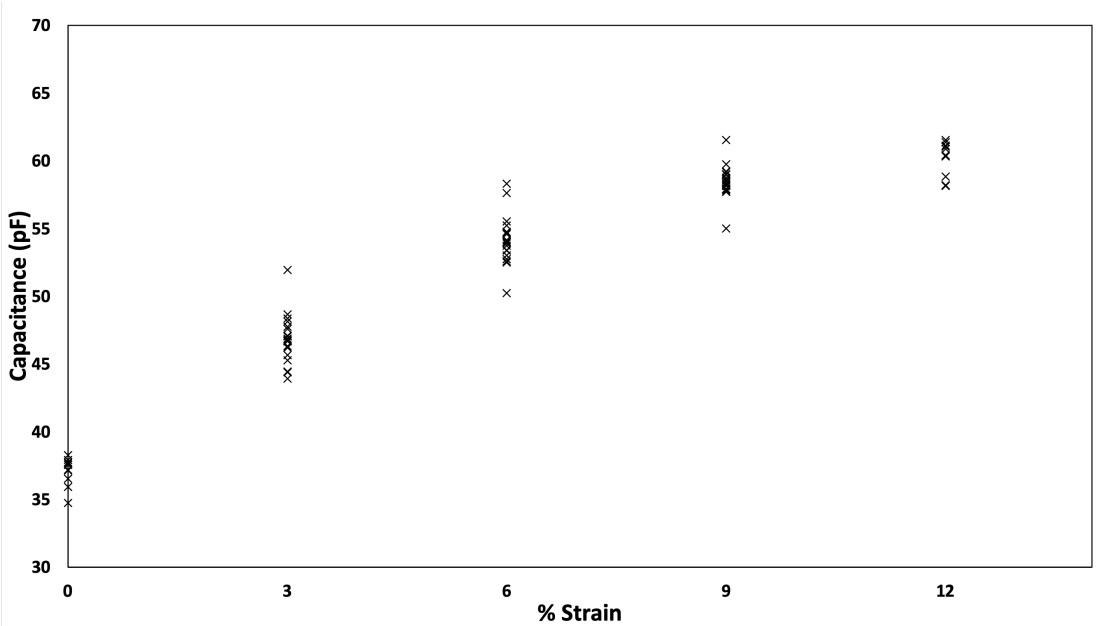

Figure 4.22: Data acquired from the LCS at different percentages of stretching in the dynamic test.

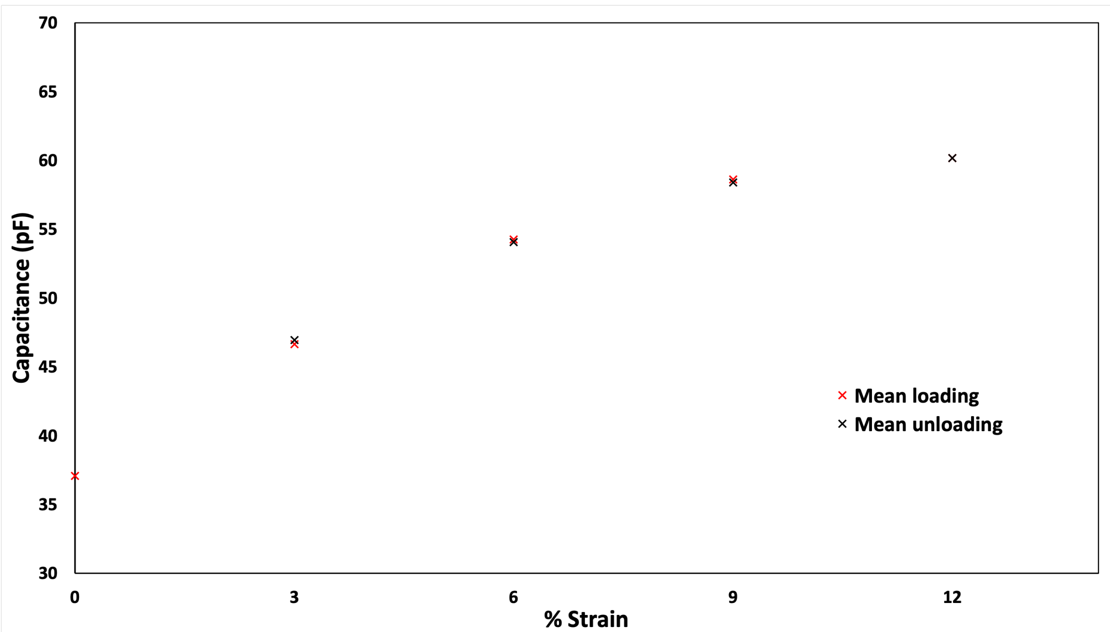

Figure 4.23: Mean of loading and unloading cycles acquired from LCS at different percentages of stretching in the dynamic test.

4.4.1.6 LTS sensor dynamic test

Table 4.10 and Figure 4.24 shows all the capacitance values acquired during the 10 cycles of the dynamic stretching test. Figure 4.25 shows all the data acquired during the semi-static test, It is possible to see how the sensor behaves in response to a faster stretching than the one tested in the semi-static test. Figure 4.26 shows the mean values in the loading and unloading cycles. From this graph is possible to see that the LTS sensor presents less hysteresis than the semi-static test. Indeed the hysteresis absolute values are 1.90, 1.40 and 2.50 pF for 3%,6%, and 9%. The higher value of standard deviation was found in 6% of stretching during the loading cycles with a value of 3.07 pF and in 3% in the unloading cycles with a value of 2.59 pF. If evaluated in percentage of the range of values the hysteresis was 4.08%, 3.00% and 5.37% for 3, 6 and 9% of stretching.
For this sensor also 3 samples from the same "Gcode" file were printed in order to test the reliability of the sensor in the dynamic stretching test. The results related to the hysteresis and the standard deviation are similar, in particular, the other two sensors presented 0.80, 1.50 and 0.80 pF and 0.60, 0.20 and 1.6 0pF of hysteresis for 3%, 6% and 9% of stretching. In percentage of the range the hysteresis values are 3.20%, 6.00%, 3.20% and 2.16%, 0.72%, 5.76%. For one sample the higher values of standard deviation were 1.44 pF for the 3% of stretching during the unloading cycles and 1.41 pF for 9% during the loading cycles, for the other sample were 1.69 pF at 6% in the unloading cycles and 1.43 pF at 3% in the unloading cycles.

%	Cyc 1	Cyc 2	Cyc 3	Cyc 4	Cyc 5	Cyc 6	Cyc 7	Cyc 8	Cyc 9	Cyc 10
0	29.4	29.7	29.3	30.4	30.3	29.8	30.1	31.2	30.5	30.1
3	41.2	41.9	39.7	38.4	42.6	43.3	40.0	41.9	39.7	38.9
6	55.1	59.4	55.1	50.0	57.6	58.3	60.5	58.0	59.6	57.9
9	66.0	63.9	66.6	64.4	69.4	64.3	68.0	68.2	69.0	69.4
12	71.3	71.6	70.9	63.2	73.6	73.0	75.9	73.8	73.0	74.3
9	68.0	69.2	70.1	69.3	69.6	70.5	68.3	67.4	68.9	72.6
6	58.0	58.5	58.3	57.4	61.7	56.5	58.8	59.2	58.5	59.0
3	42.6	41.3	40.7	43.4	48.0	39.5	42.1	46.3	42.4	41.1

Table 4.10: Capacitance values in pF of LTS at different percentages of stretching in the dynamic test.

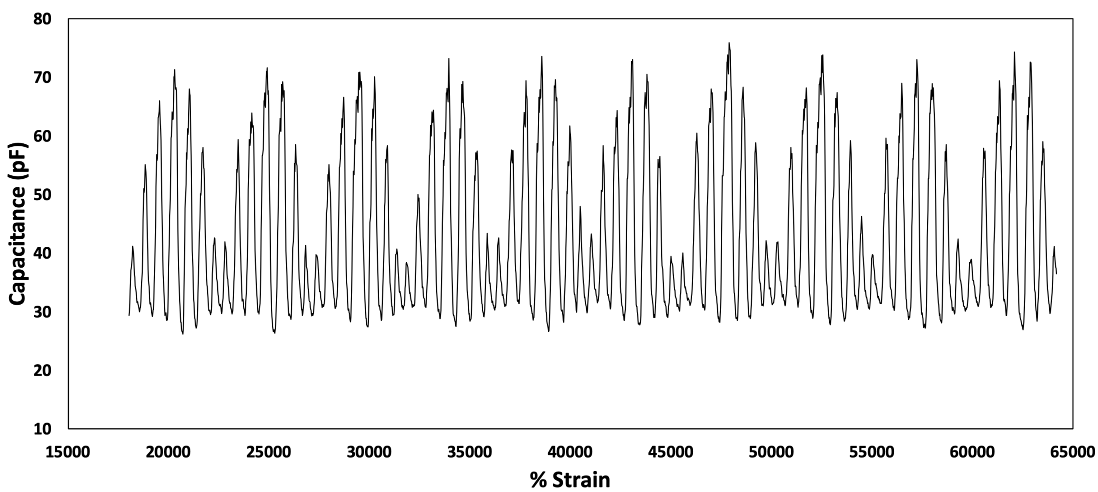

Figure 4.24: Data acquired from the LTS in the dynamic test.

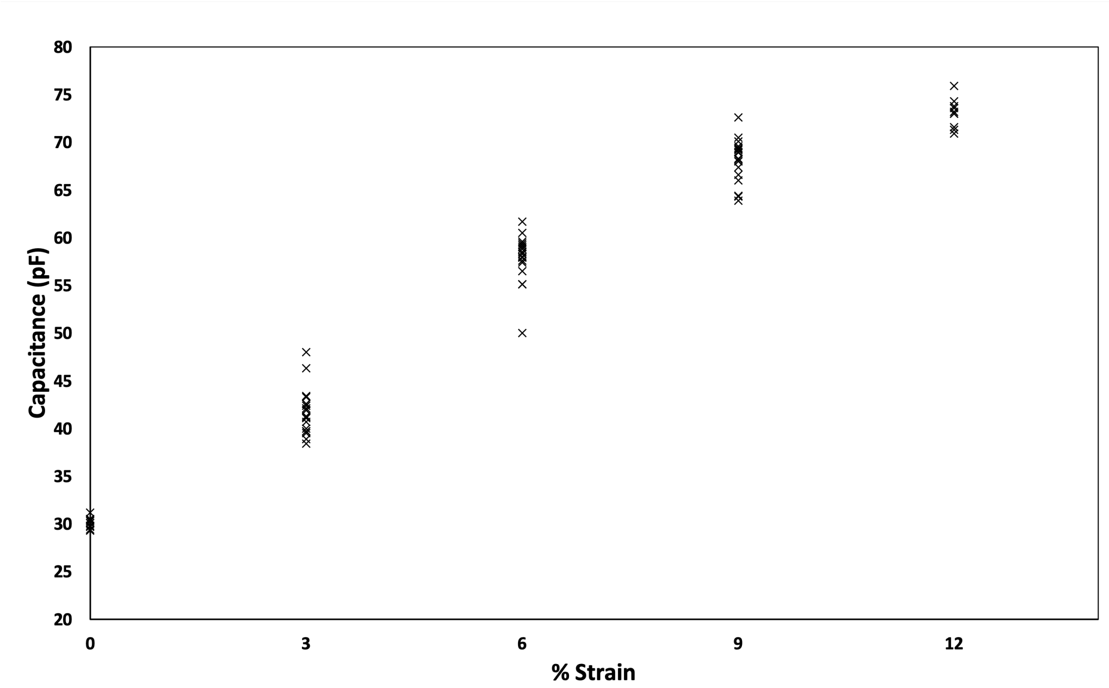

Figure 4.25: Data acquired from the LTS at different percentages of stretching in the dynamic test.

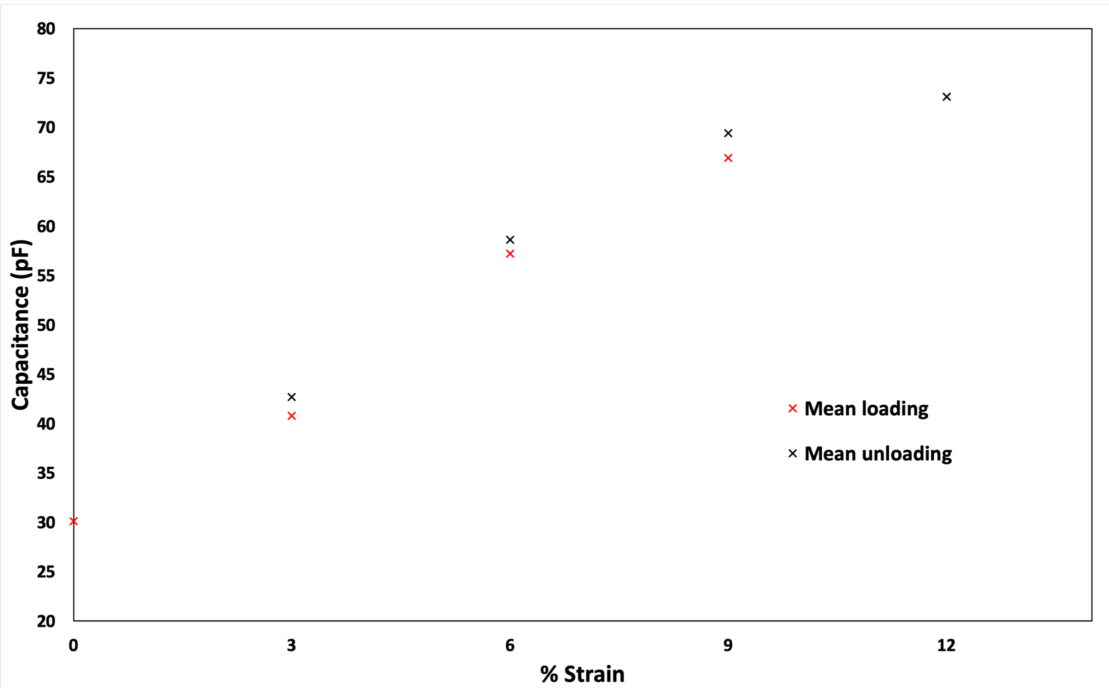

Figure 4.26: Mean of loading and unloading cycles acquired from LTS at different percentages of stretching in the dynamic test.

4.4.2 Performance validation with the hand goniometer

As described in section 3.3 the best 3D printed sensor for measuring knee ROM was chosen and then the evaluation with the hand goniometer was performed. In particular, the LTS sensor was chosen for this analysis. The LCS sensor showed better values than the LCS with less hysteresis as a percentage of the range in both semi-static and dynamic tests and better reliability (see Figure 4.16 and Figure 4.20). Even if the LCS showed better results and also appeared to be less affected by noise than the LTS, it required more strength to stretch due to the 6 layers that it is made. Since it's more difficult to stretch, when is fixed to the pants, the sensor pulls the fabric compromising its results which makes, therefore, the sensor less sensitive to the stretching. The procedure was the same used for the Adafruit, the Bendlab and IMU sensors and Figure 4.27 shows the calibration line for the LTS sensor ($y = 0.1611x^2 - 2.8248x + 8.7729$ ($R^2 = 0.982$)) and the data acquired with the capacitance voltage divider.
Figure 4.28 shows the data after the calibration process and their comparison with the "ideal" sensor response. Table 4.11 shows the results of the 10 cycles of bending with the differences between the measured angles with the hand goniometer and the LTS sensor. For the LTS the lower and the upper limit of accuracy were -15.1 and 14.3 degrees (-16.7% and 15.9% of the range), these values though are influenced by the presence of two possible outlier values in the 90 degrees of bending. If these values are not considered the lower and the upper limit of accuracy limits are -7.6 and 10.2 degrees (-8.4% and 11.3% of the range). The RMSE for the LTS including the possible outliers was 3.16 degrees. The LTS sensor was only tested until 90 degrees of bending since over that angle the sensor started pulling the pants, consequently, the sensor wasn't stretched.

Deg	Cyc 1	Cyc 2	Cyc 3	Cyc 4	Cyc 5	Cyc 6	Cyc 7	Cyc 8	Cyc 9	Cyc 10
0	3.9	-1.2	2.3	-1.5	1.1	0.3	-1.1	0.5	-0.8	0.9
10	-3.3	2.5	1.3	-4.3	4.3	-1.3	1.5	0.5	-0.7	0.5
20	-3.0	-2.3	2.6	4.4	-2.3	-0.7	1.8	1.2	0.7	-3
30	-0.8	-7.2	10	-3.7	0.9	-1.8	-0.4	1.3	-0.9	3.7
40	-2.0	-3.1	5.8	-1.1	-1.1	3.8	0.6	0.5	-4.3	-1.6
50	-0.2	2.4	-0.6	0.6	1.9	-2.5	3.1	0.7	-3.8	3.8
60	-3.4	4.0	-2.7	-0.6	5.3	-6	2.6	3.4	-7.2	3.2
70	-4.0	3.6	0.7	8.9	3.1	-7.6	-8	5	2.2	1.5
80	-4.6	0.7	1.5	3.1	3.1	-1.5	1.5	-3.1	0.8	2.3
90	-5.4	-15.8	15	6.4	-2.4	-0.8	3.2	-4.8	1.6	2.4

Table 4.11: Angles of bending measured with hand goniometer and relative deviations with degrees measured by the LTS sensor.

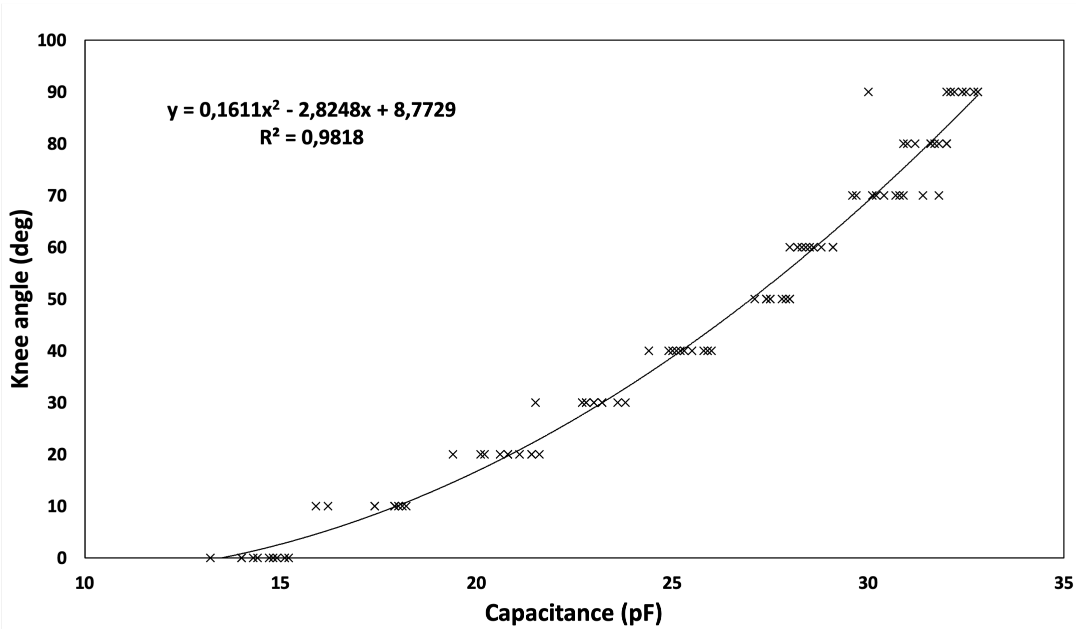

Figure 4.27: Calibration line extracted from data acquired with Arduino UNO board, the capacitance values are on the x-axis and the measured knee angles on the y-axis.

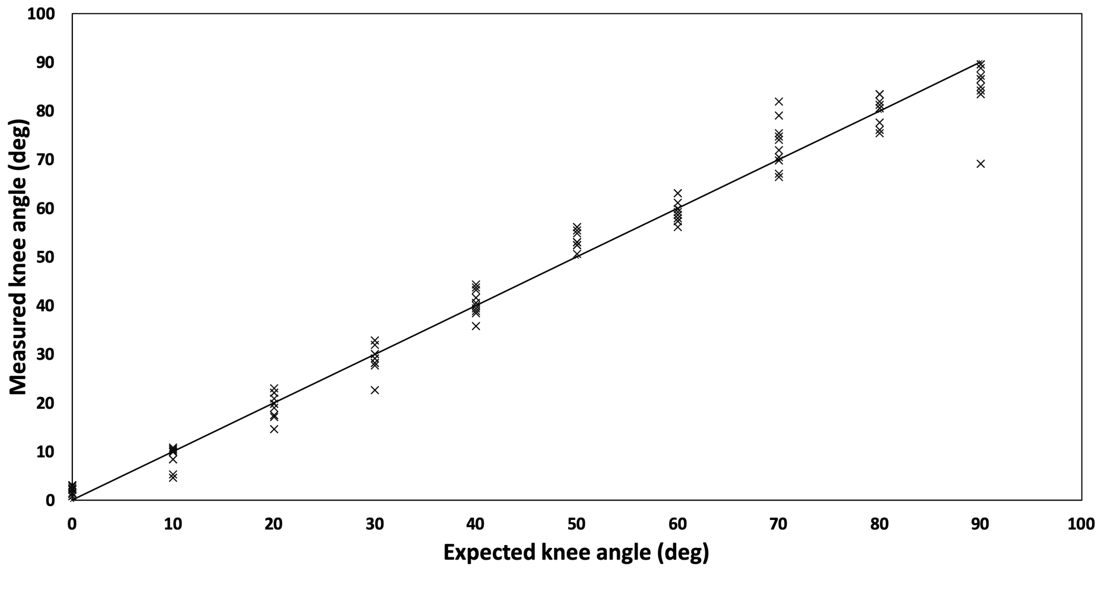

Figure 4.28: Expected knee angle vs measured knee angle for the LTS.

4.4.3 Performance validation with the IMUs

4.4.3.1 Squat test

As described in section 3.4.4 the LTS sensor, chosen as the best one for this test, was compared in a squat and gait test with the IMUs. Figure 4.29 shows the 9 squats performed by a subject and the relative angle of knee bending acquired by the IMUs and the LTS sensor. Table 4.12 shows the difference of the knee angles measured at the peaks of bending, in this case, the RMSE at the peaks was 4.26 degrees.

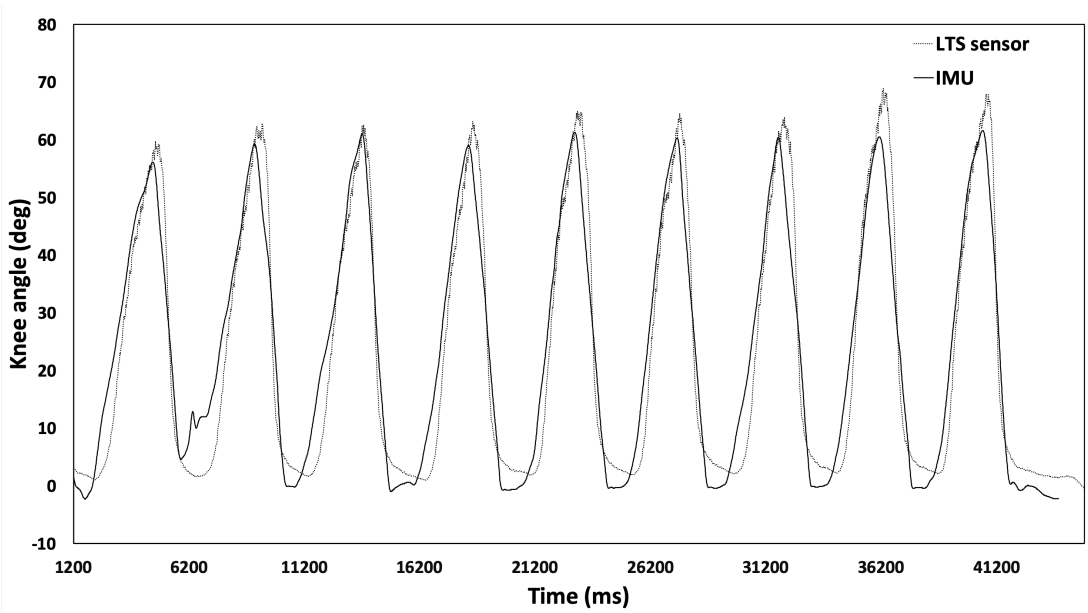

Figure 4.29: Performance validation between LTS and IMUs in the squat test.

Peak	IMU	LTS	DEV
1	56.1	58.4	2.3
2	61.0	61.9	0.9
3	59.0	62.1	3.1
4	61.3	63.2	1.9
5	60.3	64.6	4.3
6	60.4	64.6	4.2
7	60.4	63.6	3.2
8	60.5	68.9	8.4
9	61.6	66.8	5.2

Table 4.12: Differences at peaks of knee bending between IMUs and LTS in the squat test.

4.4.3.2 Gait test

The gait test was performed and also in this case, the performance were evaluated at the peaks of bending. The RMSE was calculated at the peaks of bending and the value was 5.86 degrees. Figure 4.30 shows all the data acquired by both IMUs and LTS during the gait test. It's possible to see how the LTS follows the pattern of the IMUs at peaks of bending but presents some problems when the knee angle decrease. One possible explanation of this behavior is that when the knee return to the maximum extension the sensor remain bent since it pulls the pants during the flexion.

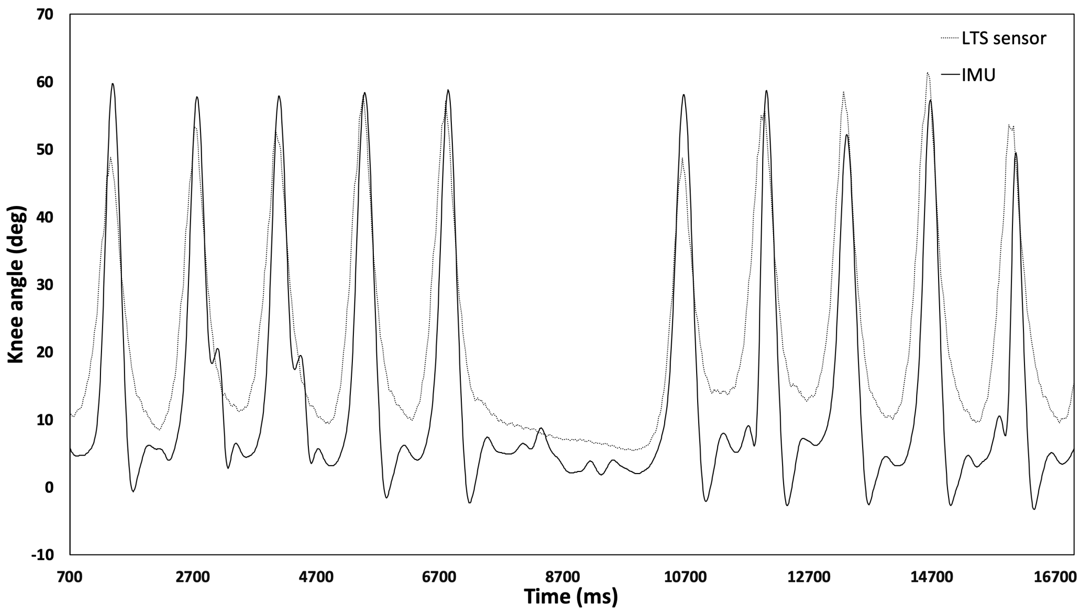

Figure 4.30: Performance validation between LTS and IMUs in the gait test.

Peak	IMU	LTS	DEV
1	59.7	48.8	10.9
2	57.8	53.3	4.5
3	57.9	52.9	5.0
4	58.4	58.0	0.4
5	58.8	57.1	1.7
6	58.1	48.7	9.4
7	58.7	55.1	3.6
8	52.2	58.6	6.4
9	57.3	61.4	4.1
10	49.5	53.6	4.1

Table 4.13: Differences at peaks of knee bending between IMUs and LTS in the gait test.

4.4.4 Performance validation with the MCS

4.4.4.1 Squat test

A Figure 4.31 shows the 9 squats performed by a subject and the relative angle of knee bending acquired by the MCS and the LTS sensor. Table 4.14 shows the difference of the knee angles measured at the peaks of bending, in this case the RMSE at the peaks was 1.83 degrees.

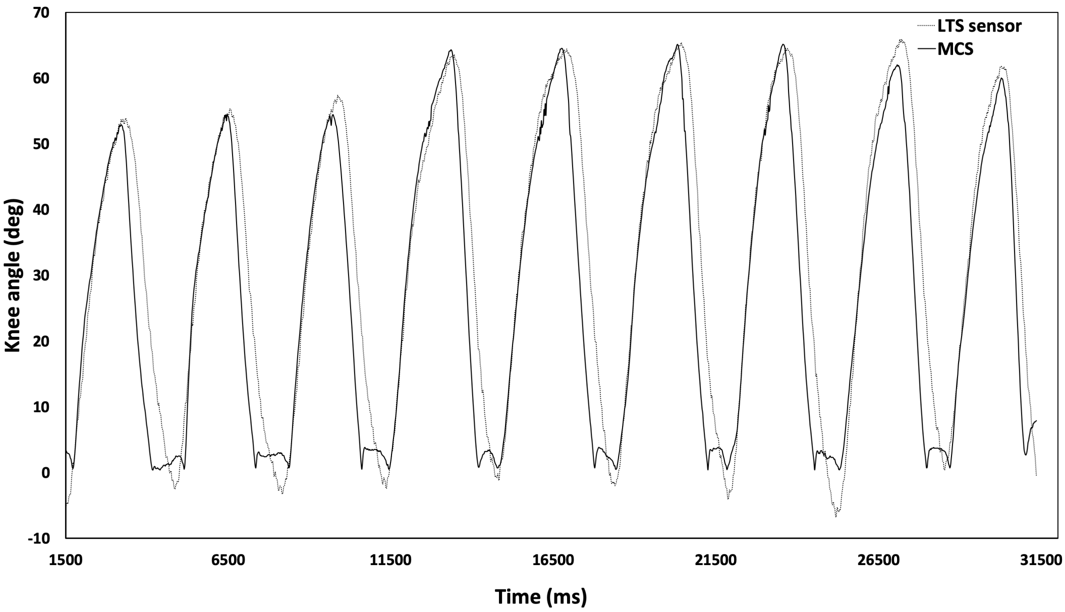

Figure 4.31: Performance validation between LTS and MCS in the squat test.

Peak	LTS	MCS	DEV
1	53.9	52.9	1.0
2	55.3	54.4	0.9
3	57.4	54.4	3.0
4	63.6	64.3	-0.7
5	64.4	64.5	-0.1
6	65.0	65.1	-0.1
7	64.6	65.1	-0.5
8	65.9	62.0	3.9
9	61.8	60.0	1.8

Table 4.14: Differences at peaks of knee bending between MCS and LTS in the squat test.

4.4.4.2 Gait test

Figure 4.32 shows the gait test performed by a subject and the relative angle of knee bending acquired by the MCS and the LTS sensor. Table 4.15 shows the difference of the knee angles measured at the peaks of bending, in this case the RMSE at the peaks was 6.44 degrees. Also in this case, the sensor presented good responses at the peaks of the knee flexion but not during the extension. It is possible to see that sometimes the sensor reaches negative angles, moreover during the extension of the knee the sensor appears to be in delay compared to the MCS. Indeed the slope of the curve after the peak is less than the slope of the MCS curve.

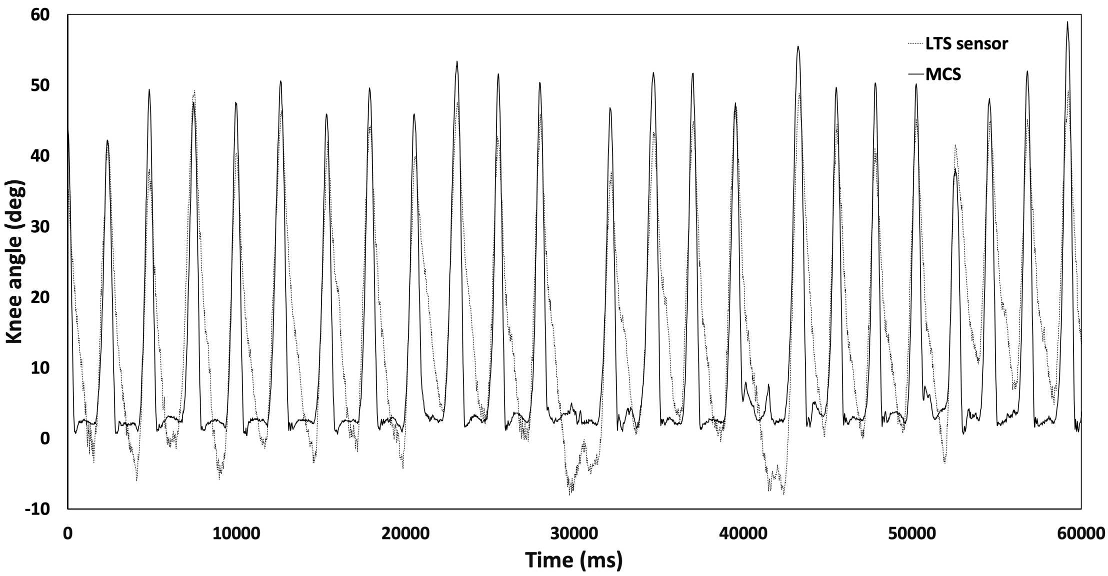

Figure 4.32: Performance validation between MSC and LTS in the gait test.

Peak	LTS	MCS	DEV
1	42.0	42.2	-0.2
2	38.1	49.4	-11.3
3	49.2	47.6	1.6
4	40.3	47.6	-7.3
5	46.4	50.6	-4.2
6	42.2	45.8	-3.6
7	44.0	49.6	-5.6
8	39.9	45.9	-6.0
9	47.6	52.7	-5.1
10	42.7	51.6	-8.9
11	45.9	50.4	-4.5
12	37.7	46.8	-9.1
13	43.4	51.8	-8.4
14	44.9	51.7	-6.8
15	46.3	47.5	-1.2
16	48.8	55.5	-6.7
17	44.4	49.7	-5.3
18	41.1	50.3	-9.2
19	45.2	50.2	-5.0
20	41.6	38.2	3.4
21	44.9	48.1	-3.2
22	45.2	52.0	-6.8
23	49.2	59.0	-9.8

Table 4.15: Differences at peaks of knee bending between MCS and LTS in the gait test.

Chapter 5

Critical analysis of results

5.1 Discussion

This master thesis project aimed to design a stretchable and flexible sensor, completely 3D printed and insertable into garments, able to detect knee joint motion. The performance of the sensor were validated with IMU and an optical system. The sensor was printed in different shapes to find the best solution in terms of accuracy and low hysteresis. Both capacitive and resistive sensors were tested. The resistive sensors appeared to be very sensitive for little percentages of stretching but after 5% of stretching the values started to be constant. Moreover in the literature was found that capacitive sensors are more reliable and less sensitive to environmental conditions like humidity and temperature variations [29]. For these reasons, we decided to continue our study developing capacitive sensors. Two different lengths of capacitive sensors were printed (9.5 inches and 11.75 inches) and for the longer one two different thicknesses were tested (3 layers and 6 layers). From the results, it's possible to confirm that the performance of the longer sensors are better since they present less hysteresis and less standard deviation. For these reasons, the 11.75 inches long thin sensor (LTS) was chosen for the analysis of the human body. The LTS with a total of three layers of thickness (1.77 inches/0.45 mm) was fixed on stretchable pants and both gait and squat tests were performed. The results showed that the angles measured by the stretchable sensors were comparable to the IMU results in both the tests. Better results have been found for the squat tests since both maximum differences and RMSE were lower that the gait tests. For what concerns the gait test, the stretch sensor wasn't able to regain a zero condition. This behavior can be seen in the lack of a little peak between each step. The validation results of the LTS with the optical system showed very promising results in the squat test with an RMSE of 1.8 degrees. For the gait test instead, the sensor presented some problems in returning to zero and the peak's RMSE was higher than the squat test (6.4 degrees).

In conclusion, the possibility of customizable length is one of the most important features of the 3D printed sensor offering the opportunity to create a model that fits perfectly each patient. Other important features are the low-cost of the sensors' materials (the sensor itself cost less than 0.10 dollars) and their lightness (less than 3 g). All these advantages allow the subject to bring home the sensor and hence to collect data during every-day life. The current methods used to detect joints motion like IMU, optical systems and rigid sensors, are in general expensive and appropriate facilities are required, forcing the patient to go to the clinic. Wearable sensors that can be inserted in garments offer the possibility to detect the day-life activities of the patients, increasing the obtainable data on the recovery status and with the use of a smartphone App offer daily feedback for both patients and physiotherapists. With the possibility to bring home the sensors, the physiotherapists can assign exercises with daily specific goals that can be achieved precisely by the patient. Daily ROM monitoring in patients after injury or surgery allows a more effective follow-up treatment and increases patient engagement by providing real-time feedback. The combination of improved and optimized rehab regimens with increased patient engagement can translate in faster recovery and lower healthcare costs.

5.2 Limitations

One of the main limitations of the sensor consists of the printing process. Even with the printer settings showed in Section 3.4 the filaments sometimes remain stuck in the nozzle. This behavior is shown usually by the conductive filaments and causes problems especially when the printer has to change from the conductive to the non-conductive material. Indeed if the nozzle is not completely clean some conductive material is printed where there shouldn't be, causing sensor noise or even shorting the circuit. These problems reflect in the printing time since the user has to pause the printer and clean manually the nozzle. Another limitation of the sensor is the conductivity of the filament, indeed to obtain a very reliable sensor the conductivity throughout all the roll of the filament has to be constant. If the filament is not completely constant in its conductivity, the printed sensors will result different from each other, sometimes making very difficult the calibration process due to very low values of capacitance. Another limitation consists in the stretchable properties, indeed the materials used to print these sensors was TPU, which is not an elastic material. The non-elastic feature of the material causes hysteresis in the sensor data and decreases its sensibility since it pulls the pants when the knee is bent.

5.3 Future developments

To make the sensor more precise one of the first things to improve should be the material used for the conductive pattern. One solution could be producing the materials directly in the lab, with a constant check on all the materials that make the filament. With the use of an extruder is possible to create the filament from the pellets of the materials, therefore, controlling that the conductivity is constant throughout the entire roll. For the contamination due to the switching of materials in the same nozzle, the solution could be to use a double nozzle printer. In fact, if the non-conductive and conductive filaments were printed from different nozzles, the contamination problem would be drastically reduced. Moreover, the printing time would be reduced since the purge volumes would not be needed anymore. Another improvement could be changing the materials from TPU to an elastic material. This switching is not easy since the printing processes is very difficult with the elastic materials. The more the filament is flexible the more it is probable that the filament remains stuck inside the nozzle. This happens because the filament has to be pushed from a gear in the nozzle and hence, if the filament is too flexible, sometimes it doesn't offer enough resistance to the pushing of the gear and remains tangled. However, if this problem were solved, it would be possible to obtain a sensor that presents a reduce hysteresis, a better sensibility and remains perfectly attached to the pants following every movement of the patient.

Bibliography

[1] S. Noll, J. Craig Garrison, J. Bothwell, and J. E. Conway, "Knee extension range of motion at 4 weeks is related to knee extension loss at 12 weeks after anterior cruciate ligament reconstruction," *Orthopaedic Journal of Sports Medicine*, vol. 3, no. 5, pp. 1–6, 2015.

[2] F. R. Noyes, R. E. Mangine, and S. Barber, "Early knee motion after open and arthroscopic anterior cruciate ligament reconstruction," *The American Journal of Sports Medicine*, vol. 15, no. 2, pp. 149–160, 1987.

[3] B. A. Bousquet, L. O'Brien, S. Singleton, and M. Beggs, "Post-Operative Criterion Based Rehabilitation of Acl Repairs: a Clinical Commentary," *International Journal of Sports Physical Therapy*, vol. 13, no. 2, pp. 293–305, 2018.

[4] S. van Grinsven, R. E. van Cingel, C. J. Holla, and C. J. van Loon, "Evidence-based rehabilitation following anterior cruciate ligament reconstruction," *Knee Surgery, Sports Traumatology, Arthroscopy*, vol. 18, no. 8, pp. 1128–1144, 2010.

[5] T. SHAW, "A users guide to outcome measurement following ACL reconstruction," *Physical Therapy in Sport*, vol. 5, no. 2, pp. 57–67, 2004.

[6] A. Biggs, W. L. Jenkins, S. E. Urch, and K. D. Shelbourne, "Rehabilitation for Patients Following ACL Reconstruction: A Knee Symmetry Model.," *North American journal of sports physical therapy : NAJSPT*, vol. 4, no. 1, pp. 2–12, 2009.

[7] J. T. Cavanaugh and M. Powers, "ACL Rehabilitation Progression: Where Are We Now?," *Current reviews in musculoskeletal medicine*, vol. 10, no. 3, pp. 289–296, 2017.

[8] T. A. Lentz, G. Zeppieri, S. M. Tillman, P. A. Indelicato, M. W. Moser, S. Z. George, and T. L. Chmielewski, "Return to Preinjury Sports Participation Following Anterior Cruciate Ligament Reconstruction: Contributions of Demographic, Knee Impairment, and Self-report Measures," *Journal of Orthopaedic & Sports Physical Therapy*, vol. 42, no. 11, pp. 893–901, 2012.

[9] S. D. Barber-Westin and F. R. Noyes, "Objective criteria for return to athletics after anterior cruciate ligament reconstruction and subsequent reinjury

rates: a systematic review.," *The Physician and sportsmedicine*, vol. 39, no. 3, pp. 100–110, 2011.

[10] J. Kvist, "Rehabilitation Following Anterior Cruciate Ligament Injury," vol. 34, no. 4, pp. 269–280, 2004.

[11] M. Henriksson, P. Rockborn, and L. Good, "Range of motion training in brace vs. plaster immobilization after anterior cruciate ligament reconstruction: a prospective randomized comparison with a 2-year follow-up," no. 1990, pp. 73–80, 2002.

[12] M. A. Risberg, I. Holm, H. Steen, J. Eriksson, and A. Ekeland, "The effect of knee bracing after anterior cruciate ligament reconstruction: A prospective, randomized study with two years' follow-up," *American Journal of Sports Medicine*, vol. 27, no. 1, pp. 76–83, 1999.

[13] T. Muellner, Y. Alacamlioglu, A. Nikolic, and R. Schabus, "No benefit of bracing on the early outcome after anterior cruciate ligament reconstruction," *Knee Surgery, Sports Traumatology, Arthroscopy*, vol. 6, no. 2, pp. 88–92, 1998.

[14] S. D. Barber-Westin and F. R. Noyes, "Factors used to determine return to unrestricted sports activities after anterior cruciate ligament reconstruction," *Arthroscopy - Journal of Arthroscopic and Related Surgery*, vol. 27, no. 12, pp. 1697–1705, 2011.

[15] T. A. Lentz, S. M. Tillman, P. A. Indelicato, M. W. Moser, S. Z. George, and T. L. Chmielewski, "Factors associated with function after anterior cruciate ligament reconstruction," *Sports Health*, vol. 1, no. 1, pp. 47–53, 2009.

[16] K. Donald Shelbourne and T. Gray, "Anterior cruciate ligament reconstruction with autogenous patellar tendon graft followed by accelerated rehabilitation. A two- to nine-year followup," *American Journal of Sports Medicine*, vol. 25, no. 6, pp. 786–795, 1997.

[17] K. I. M. Do Kyung, H. Ji Hye, and P. Won Hah, "Effects of 4 weeks preoperative exercise on knee extensor strength after anterior cruciate ligament reconstruction," *Journal of Physical Therapy Science*, vol. 27, no. 9, pp. 2693–2696, 2015.

[18] A. L. Miner, E. A. Lingard, E. A. Wright, C. B. Sledge, J. N. Katz, W. Gillespie, C. Howie, I. Annan, P. Abernathy, A. Gibson, J. Lane, I. Pinder, D. Weir, N. Brewster, K. Bettinson, M. Needhoff, R. Jackson, T. Wilton, P. Howard, I. Forster, P. Szyprt, C. Moran, D. Whitaker, M. Bullock, Z. Hinchcliffe, I. Learmonth, J. Newman, C. Ackroyd, G. Langkamer, R. Spencer, M. Shannon, E. Smith, J. Dixon, S. Whitehouse, F. Ewald, R. Poss, J. Wright, S. Martin, J. Kwon, Y. Valderrama, S. Harwin, M. Lichardi, M. Mehlhoff, L. Weiler, T. Cahalan, R. Cronk, A. Sandago, S. Rackermann, E. McLaughlin, P. Lewis,

R. Bauze, T. Stevenson, G. Morrison, and J. Clasohm, "Knee range of motion after total knee arthroplasty: How important is this as an outcome measure?," *Journal of Arthroplasty*, vol. 18, no. 3, pp. 286–294, 2003.

[19] P. Gibbs and H. H. Asada, "Wearable conductive fiber sensors for measuring joint movements," *Proceedings - IEEE International Conference on Robotics and Automation*, vol. 2004, no. 5, pp. 4753–4758, 2004.

[20] E. Papi, Y. N. Bo, and A. H. McGregor, "A flexible wearable sensor for knee flexion assessment during gait," *Gait and Posture*, vol. 62, no. October 2017, pp. 480–483, 2018.

[21] L. Sbernini, A. Pallotti, and G. Saggio, "Evaluation of a Stretch Sensor for its inedited application in tracking hand finger movements," *2016 IEEE International Symposium on Medical Measurements and Applications, MeMeA 2016 - Proceedings*, no. Memea, 2016.

[22] A. Tognetti, F. Lorussi, G. D. Mura, N. Carbonaro, M. Pacelli, R. Paradiso, and D. D. Rossi, "New generation of wearable goniometers for motion capture systems," *Journal of NeuroEngineering and Rehabilitation*, vol. 11, no. 1, pp. 1–17, 2014.

[23] H. Jiyong, Z. Xiaofeng, L. Guohao, Y. Xudong, and D. Xin, "Electrical properties of PPy-coated conductive fabrics for human joint motion monitoring," *Autex Research Journal*, vol. 16, no. 1, pp. 7–12, 2016.

[24] T. W. Shyr, J. W. Shie, C. H. Jiang, and J. J. Li, "A textile-based wearable sensing device designed for monitoring the flexion angle of elbow and knee movements," *Sensors (Switzerland)*, vol. 14, no. 3, pp. 4050–4059, 2014.

[25] S. I. Lee, J. F. Daneault, and L. Weydert, "A novel flexible wearable sensor for estimating joint-angles," *BSN 2016 - 13th Annual Body Sensor Networks Conference*, pp. 377–382, 2016.

[26] T.-L. R. Zhen Yang, Yu Pang, Xiao-lin Han, Yifan Yang, Jiang Ling, Muqiang Jian, Yingying Zhang, Yi Yang, "Graphene Textile Strain Sensor with Negative Resistance Variation for Human Motion Detection.pdf," 2018.

[27] J. S. H. Yu Ra Jeong , Heun Park , Sang Woo Jin , Soo Yeong Hong , Sang-Soo Lee, "Highly Stretchable and Sensitive Strain Sensors Using Fragmentized Graphene Foam.pdf," 2015.

[28] B. Huang, M. Li, T. Mei, D. McCoul, S. Qin, Z. Zhao, and J. Zhao, "Wearable stretch sensors for motion measurement of the wrist joint based on dielectric elastomers," *Sensors (Switzerland)*, vol. 17, no. 12, 2017.

[29] L. B. Massimo Totaro, Tommaso Poliero, Alessio Mondini , Chiara Lucarotti, Giovanni Cairoli, Jesùs Ortiz, "Soft Smart Garments for Lower Limb Joint.pdf," 2017.

[30] C. R. Walker and I. A. Anderson, "Monitoring diver kinematics with dielectric elastomer sensors," *Electroactive Polymer Actuators and Devices (EAPAD) 2017*, vol. 10163, p. 1016307, 2017.

[31] M. Alsharari, B. Chen, and W. Shu, "3D Printing of Highly Stretchable and Sensitive Strain Sensors Using Graphene Based Composites," *Proceedings*, vol. 2, no. 13, p. 792, 2018.

[32] J. Z. Gul, M. Sajid, and K. H. Choi, "3D printed highly flexible strain sensor based on TPU-graphene composite for feedback from high speed robotic applications," *Journal of Materials Chemistry C*, vol. 7, no. 16, pp. 4692–4701, 2019.

[33] K. Li, H. Wei, W. Liu, H. Meng, P. Zhang, and C. Yan, "3D printed stretchable capacitive sensors for highly sensitive tactile and electrochemical sensing," *Nanotechnology*, vol. 29, no. 18, pp. 1–7, 2018.

[34] G. E. Hancock, T. Hepworth, and K. Wembridge, "Accuracy and reliability of knee goniometry methods," *Journal of Experimental Orthopaedics*, vol. 5, no. 1, 2018.

[35] Y. Koyama, M. Nishiyama, and K. Watanabe, "Wearable motion capturing with the flexing and turning based on a hetero-core fiber optic stretching sensor," *21st International Conference on Optical Fiber Sensors*, vol. 7753, p. 77534B, 2011.

Aknowledgments

First, I would like to thank Dr. Fabrizio Billi for hosting me 6 months in his laboratory at UCLA, Los Angeles, for having being such a great mentor and for allowing me to grow up both professionally and personally. I would like to thank Prof. Laura Gastaldi for agreeing to have been my supervisor here in Italy. I would also like to thank my parents and my grandfather for giving me both economic and moral support for making me living this amazing experience that I will never forget. I would like to thank Giulia for having been always next to me not only during this 6 months but also during my entire course of study, without her advice and support I would not be here now presenting this thesis. I would also thank my friends Theo, Dale, and Jeorge for welcoming me from the first moment that I arrived in Los Angeles and never haven't made me feel alone.

In primo luogo, vorrei ringraziare il Prof. Fabrizio Billi per avermi ospitato 6 mesi nel suo laboratorio presso UCLA, a Los Angeles, per essere stato un eccellente guida e per avermi dato l'opportunità di crescere sia professionalmente che personalmente. Vorrei ringraziare la Prof. Laura Gastaldi per aver accettato di essere il mio supervisore qui in Italia. Vorrei anche ringraziare i miei genitori e mio nonno per avermi fornito un sostegno sia economico che morale per farmi vivere questa straordinaria esperienza che non dimenticherò mai. Vorrei ringraziare Giulia per essere stata sempre accanto a me non solo durante questi 6 mesi ma anche durante tutto il mio corso di studi, senza i suoi consigli e il suo supporto, non sarei qui a presentare questa tesi. Ringrazio anche i miei amici Theo, Dale e Jeorge per avermi dato il benvenuto dal primo momento in cui sono arrivato a Los Angeles e per non avermi mai fatto sentire solo.